Astrocytic control of synaptic NMDA receptors

C. Justin Lee[1], Guido Mannaioni[2], Hongjie Yuan[3], Dong Ho Woo[1], Melissa B. Gingrich[3] and Stephen F. Traynelis[3]

[1]*Center for Neural Science, Division of Life Sciences, Korea Institute of Science and Technology, Seoul, Korea*
[2]*Department of Pharmacology, University of Florence, Florence, Italy*
[3]*Department of Pharmacology, Emory University School of Medicine, Atlanta, GA, USA*

Astrocytes express a wide range of G-protein coupled receptors that trigger release of intracellular Ca^{2+}, including P2Y, bradykinin and protease activated receptors (PARs). By using the highly sensitive sniffer-patch technique, we demonstrate that the activation of P2Y receptors, bradykinin receptors and protease activated receptors all stimulate glutamate release from cultured or acutely dissociated astrocytes. Of these receptors, we have utilized PAR1 as a model system because of favourable pharmacological and molecular tools, its prominent expression in astrocytes and its high relevance to neuropathological processes. Astrocytic PAR1-mediated glutamate release *in vitro* is Ca^{2+} dependent and activates NMDA receptors on adjacent neurones in culture. Activation of astrocytic PAR1 in hippocampal slices induces an APV-sensitive inward current in CA1 neurones and causes APV-sensitive neuronal depolarization in CA1 neurones, consistent with release of glutamate from astrocytes. PAR1 activation enhances the NMDA receptor-mediated component of synaptic miniature EPSCs, evoked EPSCs and evoked EPSPs in a Mg^{2+}-dependent manner, which may reflect spine head depolarization and consequent reduction of NMDA receptor Mg^{2+} block during subsequent synaptic currents. The release of glutamate from astrocytes following PAR1 activation may also lead to glutamate occupancy of some perisynaptic NMDA receptors, which pass current following relief of tonic Mg^{2+} block during synaptic depolarization. These results suggest that astrocytic G-protein coupled receptors that increase intracellular Ca^{2+} can tune synaptic NMDA receptor responses.

(Received 13 February 2007; accepted after revision 4 April 2007; first published online 5 April 2007)
Corresponding author S. F. Traynelis: Department Pharmacology, 5062 Rollins Research Center, 1510 Clifton Road, Atlanta, GA 30322-3090, USA. Email: strayne@ emory.edu

Astrocytes have been known for decades to express a wide range of G-protein coupled receptors (reviewed in Porter & McCarthy, 1997). However, there is no clear consensus for hypothetical roles of these receptors in CNS function. Astrocytic G-protein coupled receptors that stimulate release of Ca^{2+} from intracellular stores have recently been shown to stimulate glutamate release (e.g. Parpura *et al.* 1994; Bezzi *et al.* 1998; Araque *et al.* 2000), which has a number of important implications for neuronal signalling. We have evaluated the ability of three astrocytic receptors coupled through G-protein signalling to intracellular Ca^{2+} to release glutamate in a manner that can influence neuronal function. P2Y receptors, bradykinin receptors and protease activated receptors are widely expressed in human and rodent astrocytes as well as some neurones (Parpura *et al.* 1994; Weinstein *et al.* 1995; Ikeda *et al.* 2000; Franke *et al.* 2004; Junge *et al.* 2004; Kobayashi *et al.* 2006). Of these receptors, activation of P2Y is the best known, and has been shown to both release glutamate and potentiate NMDA receptor function (Jeremic *et al.* 2001; Wirkner *et al.* 2007). In this study we have focused on activation of protease activated receptor-1 (PAR1) in astrocytes because a number of tools exist such as selective PAR1 activators (Hollenberg *et al.* 1997), selective PAR1 inhibitors (Bernatowicz *et al.* 1996) and PAR−/− mice (Connolly *et al.* 1996). In addition, PAR1 is predominantly expressed in astrocytes over neurones (Weinstein *et al.* 1995; Junge *et al.* 2004). Cleavage of the PAR1 N-terminus (Coughlin, 2000, 2001; Macfarlane *et al.* 2001) can initiate intracellular signalling in a number of G-protein linked pathways (Ogino *et al.* 1996; Wang *et al.* 2002*a*,*b*; Wang & Reiser, 2003; Xi *et al.* 2003; James *et al.* 2005). PAR1 is functionally coupled to Gαi/o, Gα12/13 and Gαq/11. PAR1 activation in astrocytes can stimulate ERK phosphorylation and tyrosine kinase activity, as well as increase intracellular Ca^{2+} (Kahan *et al.* 1992; Zhang *et al.* 1995; Coughlin, 2000, 2001; Macfarlane *et al.* 2001; Nicole *et al.* 2005).

C. J. Lee and G. Mannaioni contributed equally to this work. This paper has online supplemental material.

DOI: 10.1113/jphysiol.2007.130377

Here we describe glial–neuronal signalling initiated by astrocytic PAR1 activation that leads to glutamate release from astrocytes and potentiation of the synaptic NMDA receptor response by a Mg^{2+}-dependent mechanism. We propose that this potentiation should operate for a wide range of astrocytic G-protein coupled receptors that can elevate intracellular Ca^{2+} (e.g. Parpura *et al.* 1994; Bezzi *et al.* 1998; Sorensen *et al.* 2003).

Methods

Tissue culture

Cultured astrocytes were prepared from P0–P3 postnatal mice. The cerebral cortex was dissected free of adherent meninges, minced and dissociated into single cell suspension by trituration through a Pasteur pipette. All procedures involving the use of animals were reviewed and approved by the Emory University IACUC. Dissociated cells were plated onto either 12 mm glass coverslips or six-well plates coated with 0.1 mg ml^{-1} poly D-lysine. Cells were grown in Dulbecco's modified Eagle's medium (DMEM; Gibco, cat. no. 11960-044) supplemented with 25 mM glucose, 10% heat-inactivated horse serum, 10% heat-inactivated fetal bovine serum, 2 mM glutamine and 1000 units ml^{-1} penicillin–streptomycin. Cultures were maintained at 37°C in a humidified 5% CO_2-containing atmosphere. Astrocyte cultures prepared in this way were previously determined by glial fibrillary acidic protein (GFAP) staining to be greater than 95% astrocytes (Nicole *et al.* 2005). In some experiments, the culture medium was replaced 24 h after plating with DMEM with all added components except glutamine, and cultures maintained for 4 days before experimentation in glutamine-free media.

For astrocyte–neurone coculture, a monolayer of wild-type astrocytes was grown to confluency (7–14 days in culture). Subsequently, the cortex from a P0 to P5 PAR1−/− mouse (Connolly *et al.* 1996) was dissected free of meninges and digested for 30 min in 1 mg ml^{-1} trypsin at 37°C. PAR1−/− mice were > 99% C57Bl/6 (> 7 backcrossings), and wild-type mice were from a colony derived from PAR1−/− littermates. All experiments were done within three generations of establishing the homozygous colony. The cortical cells were plated at low density on top of the monolayer of wild-type astrocytes. Neurones were used for Ca^{2+} imaging after 1–5 days in culture (see below). HEK 293 cells (ATCC1573) were plated onto 12 mm glass coverslips coated with 5–10 μg ml^{-1} poly D-lysine and maintained as previously described (Traynelis & Wahl, 1997; Banke *et al.* 2000). HEK 293 cells were transfected with a 1 : 3.5 ratio of green fluorescent protein (GFP) and GluR1(L497Y) using the calcium phosphate method for 6–8 h, after which the medium was replaced and supplemented with 1 mM kynurenic acid and 10 μM *N*-(4-hydroxyphenylpropanoyl) spermine or 10 μM 6-cyano-7-nitroquinoxaline-2,3-dione (CNQX). Transfected HEK cells were subsequently trypsinized and replated onto astrocyte feeder layers derived from either wild-type or PAR1−/− mice 24 h post-transfection, and recordings performed 24 h after replating.

Acute dissociation of CA1 GFAP–GFP astrocytes from hippocampal slices

The CA1 region was microdissected from hippocampal slices (300 mm thick, see below) and exposed for 30 min at 37°C to 1 mg ml^{-1} trypsin (type III; Sigma, St Louis, MO, USA) dissolved in divalent free Hepes buffered saline. Trypsin was subsequently inactivated by adding external solution containing $CaCl_2$ and $MgCl_2$. The hippocampal sections were mechanically dissociated with fire-polished glass pipettes. Cells were washed twice and plated on poly D-lysine (10 μg ml^{-1}) coated glass coverslips, and placed in an incubator for 30–60 min before use.

Perforated patch recording from cultured neurones and HEK 293 cells

Whole-cell perforated-patch recording from cultured cortical neurones or HEK cells under voltage clamp (holding potential –60 mV) was made with an Axopatch 200B amplifier (Axon Instruments, Union City, CA, USA). The recording chamber was continually perfused with recording solution composed of (mM): 150 NaCl, 3 KCl, 2 $CaCl_2$, 5.5 glucose and 10 Hepes (pH 7.4 by NaOH; osmolarity adjusted to 315–320 mosmol kg^{-1} with sucrose). Recording electrodes (4–7 MΩ) were filled with (mM): 150 $CsMeSO_4$, 10 NaCl, 0.5 $CaCl_2$, 10 Hepes and 25–50 μg ml^{-1} gramicidin D (pH adjusted to 7.3 with CsOH and osmolarity adjusted to 310 mosmol kg^{-1} with sucrose). It took 20–30 min to achieve acceptable perforation with series resistance ranging from 30 to 60 MΩ. All electrophysiological data from cultured cells in this study were collected at room temperature (23–25°C).

Electrophysiological recording from hippocampal slices

Young rats (Sprague–Dawley, age P15–20) or mice (C57/Bl6, age P14–19) were deeply anaesthetized with isoflurane and decapitated. The brain was rapidly removed and submerged in an ice-cold oxygenated artificial cerebrospinal fluid (ACSF) composed of (mM): 130 NaCl, 24 $NaHCO_3$, 3.5 KCl, 1.25 NaH_2PO_4, 1 $CaCl_2$, 3 $MgCl_2$ and 10 glucose saturated with 95% O_2–5% CO_2, at pH 7.4. The hemisected brain was glued onto the stage of a vibrating microtome (Leica VT1000S) and sections of 300 μm thickness were cut and stored in an incubation chamber at room temperature for about 1 h before use.

For voltage clamp experiments, the solution used to fill the electrodes was composed of (mM): 140 Cs-$MeSO_4$, 10 Hepes, 7 NaCl, 4 Mg-ATP and 0.3 Na_3-GTP; the solution for current clamp recordings was composed of (mM): 140 K-$MeSO_4$, 10 Hepes, 7 NaCl, 4 Mg-ATP and 0.3 Na_3-GTP and supplemented with 1 mM QX314; 1 mM QX314 was omitted from some current clamp recordings (e.g. Fig. 8*E*). Slices were placed on the stage of an upright microscope underneath a platinum and nylon restraining grid, and superfused with oxygenated ACSF at room temperature (23°C); some experiments were performed at 34°C by temperature controller (TC-344B, Warner, Hamden, CT, USA). The standard ACSF recording solution was composed of (mM): 130 NaCl, 24 $NaHCO_3$, 3.5 KCl, 1.25 NaH_2PO_4, 1.5 $CaCl_2$, 1.5 $MgCl_2$ and 10 glucose saturated with 95% O_2–5% CO_2, at pH 7.4. For some experiments 0.5–1 μM TTX, 10 μM NBQX, or 10–20 μM bicuculline was added to the extracellular solution, extracellular Mg^{2+} was reduced to 5 μM, and/or extracellular Ca^{2+} raised to 2 mM. Visually guided whole-cell patch recordings were obtained from CA1 pyramidal neurones in voltage clamp or current clamp configuration using an Axopatch 200A (Axon Instruments, Union City, CA, USA) and a borosilicate patch pipette of 5–7 MΩ resistance. All neurones included in this study had a resting membrane potential below −55 mV, had an access resistance in the range of 10–20 MΩ, and showed only minimal variation in these parameters during the recordings period. Records were filtered at 5 kHz and digitized at 20 kHz using a Digidata 1200A/D board. Synaptic responses were evoked by applying 0.1 ms current injection (1–100 μA) to a bipolar stimulating electrode placed in the stratum radiatum. Thrombin (Calbiochem) concentration was determined as described by Gingrich *et al.* (2000) using conversion of 1 U ml^{-1} = 10 nM. Selective PAR1 activating peptide TFLLR-NH_2 (TFLLR)and thrombin were applied by gravity perfusion at 1.0 ml min^{-1}, with extensive washing of perfusion lines, chamber, and objective between experiments to remove all residual thrombin, which has been reported to irreversibly cleave PAR1 at picomolar concentration. Removal of all thrombin ensured that PAR1 receptors were not precleaved by residual thrombin prior to experimentation; failure to fully wash thrombin from the system diminished or eliminated subsequent thrombin responses.

Miniature EPSC analysis

Miniature EPSCs (mEPSCs) were digitized at 10 kHz and the records were filtered with a digital Gaussian filter (−3 dB) with a cutoff frequency of 1 kHz. The mEPSCs were automatically detected and grouped based on an amplitude threshold of 10 pA and rise time between 0 and 5 (fast rise time) and 5–10 ms (slow rise time); a small number of apparent mEPSCs with rise times slower than 10 ms were not studied further. Selected mEPSCs were scaled, averaged, and fitted with a sum of two exponential functions:

$$\text{Response amplitude}(t) = \text{Amplitude}_1 \exp(-\text{time}/\tau_1) + \text{Amplitude}_2 \exp(-\text{time}/\tau_2).$$

If the first decay constant (τ_1) and the second decay constant (τ_2) were within 10%, the curve was subsequently refitted with a single exponential function. Both the frequency and the peak amplitude of detected events were analysed. The AMPA receptor blocker CNQX (10 μM) was routinely added at the end of experiments to verify that the mEPSCs were AMPA receptor-mediated. All data were acquired, stored and analysed using pCLAMP 8 (Axon Instruments) and Mini Analysis Program (Synaptosoft, Inc., Decatur, GA, USA). In all of the experiments, drugs were administered by addition to the perfusing medium and were applied for a sufficient period to allow equilibration.

Imaging of Ca^{2+}-sensitive dyes

Cultured astrocytes were incubated with 5 μM Fura-2-AM in 1 μM pluronic acid (Molecular Probes) for 30 min at room temperature, and subsequently transferred to a microscope stage for imaging. External solution contained (mM): 150 NaCl, 10 Hepes, 3 KCl, 2 $CaCl_2$, 2 $MgCl_2$, 5.5 glucose; pH adjusted to pH 7.3 and osmolarity to 325 mosmol kg^{-1}. Intensity images of 510 nm wavelength were taken at 340 nm and 380 nm excitation wavelengths using either a MicroMax Camera (Princeton Scientific Instruments, Inc., Monmouth, NJ, USA) or an intensified video camera (PTI), and the two resulting images were used for ratio calculations using Axon Imaging Workbench version 2.2.1 (Axon Instruments).

In order to evaluate Ca^{2+} signalling in neurones and glia in slices, patch electrodes were filled with (mM): 140 potassium gluconate, 10 HEPES, 7 NaCl, 4 Mg-ATP, 0.3 Na_3-GTP, and either 100 μM Fluo-3 (Kd: 390 nM) or Oregon Green 488 BAPTA-2 (K_d 580 nM). The external solution contained 1 μM TTX. Throughout the experiments −5 mV voltage steps (15 ms duration) were applied at 30 s intervals from a holding potential of −70 mV to monitor the holding current, series resistance, and membrane input resistance continuously. After entering whole-cell mode, the CA1 pyramidal cells in slices were maintained for 20 min to allow for dye filling before image acquisition using a Princeton MicroMax camera. After the baseline period, TFLLR (30–100 μM) was applied, and images were acquired every 3 s with a 25 ms exposure to 450–490 nm light for each image. Ca^{2+}-dependent fluorescence intensity (520 nm) was measured in cell bodies and processes by using Axon Imaging Workbench (v. 2.2.1) and

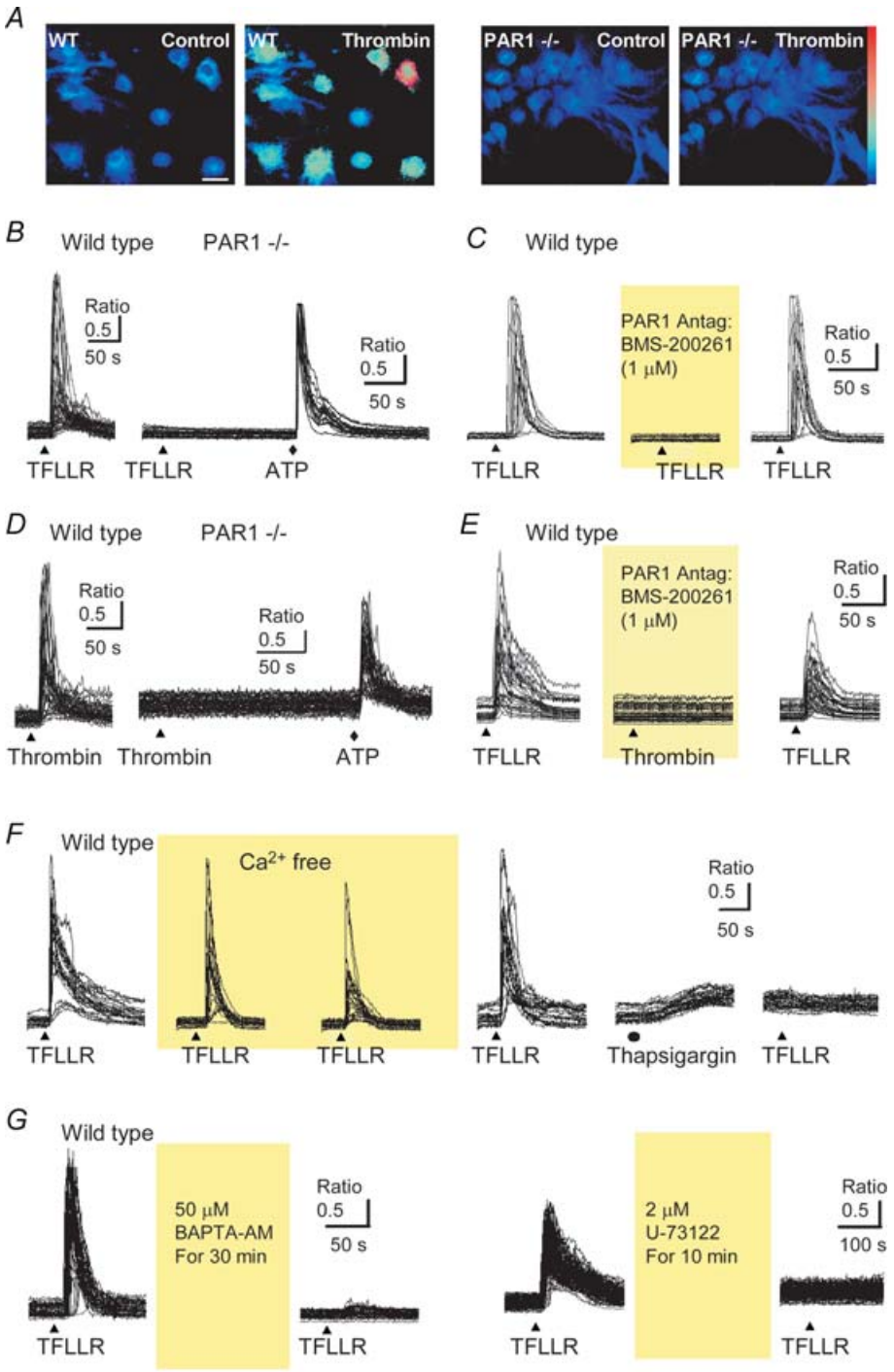

Figure 1. Cultured astrocytes express functional PAR1
A, a ratio image of Fura-2-AM loaded cultured wild-type and PAR1−/− mouse astrocytes is shown before and 20 s after 30 nM thrombin application. The colour scale shows the pseudocolour coding of ratio values ranging from 0 (bottom) to 3 (top); calibration bar is 50 μm. *B*, superimposed representative ratio response time courses show magnitude of the changes in Fura-2 fluorescence ratio of individual wild-type and PAR1−/− astrocytes. Bath perfusion with 30 μM TFLLR for 10 s is indicated as a filled triangle; TFLLR was applied at 10 min intervals to minimize desensitization. TFLLR application did not cause a significant increase in intracellular Ca^{2+} concentration in PAR1−/− astrocytes, although astrocytes still responded to ATP as a positive control. *C*, 1 μM of the PAR1 antagonist BMS 200261 reversibly and completely antagonized the TFLLR effects on wild-type astrocytes. *D*, representative traces of Fura-2 ratio of wild-type and PAR1−/− astrocytes by 30 nM thrombin. Thrombin application did not cause a significant increase in intracellular Ca^{2+} concentration in PAR1−/− astrocytes, although astrocytes still responded

expressed as the ratio image of $(F - F_0)/F_0$, where F_0 is the fluorescence intensity before drug treatment. Increases in fluorescence ratio greater than 0.2 were considered to be significant changes; baseline fluorescence values possessed a peak $(F - F_0)/F_0$ ratio on average of 0.01 ± 0.01.

Glutamate release assay

Astrocytes were loaded with 0.5 μM L-[^{3}H]glutamate for 60 min by adding 1 μM of 1 mCi ml^{-1} L-[^{3}H]glutamate stock solution to 2 ml of culture medium. The cultures were preincubated for 30 min with 1 mM amino-oxyacetic acid and 0.5 mM methionine sulfoximine before adding [^{3}H]glutamate, and during the loading to inhibit the metabolism of glutamate to glutamine and other metabolites (Farinelli & Nicklas, 1992). Cells were washed with external solution 3 times. In some experiments, the external solution was supplemented with 50 μM L-transpyrrolidine-2,4-dicarboxylic acid (*trans*-PDC) to block glutamate transporter, a maximally effective concentration (6× IC_{50} of 4–8 μM; Mitrovic & Johnston, 1994) that is well below that suggested to stimulate heteroexchange (0.2 mM; Volterra *et al.* 1996; Bezzi *et al.* 1998). Agonists were added to external solution for 6 min and the experiment was terminated by collection of the solution. Each experimental run included the control condition in which no agonist was added. Six replicates were obtained for each drug condition. For analysis, the average radioactivity count was obtained from six replicates for each condition and compared to the average of control.

Results

Activation of PAR1 in cultured astrocytes elevates intracellular Ca^{2+}

Astrocytes express a number of G-protein coupled receptors that mediate Ca^{2+} release from intracellular stores in astrocytes maintained *in vitro*. For example, activation of protease activated receptor-1 (PAR1), bradykinin receptors, and P2Y receptors by bath perfusion of agonists increases astrocytic intracellular Ca^{2+} (see online supplemental material, Supplementary Fig. 1) in cultures that were determined to be > 95% astrocytic on the basis of both GFAP staining and lack of NMDA receptor responses (Nicole *et al.* 2005). In this study we have focused on PAR1, which is strongly expressed in astrocytes in rodent (e.g. Meli *et al.* 2001; Wang *et al.* 2002*a*,*b*; Sorensen *et al.* 2003; Suo *et al.* 2004) as well as in human brain tissue (Junge *et al.* 2004; Hamill *et al.* 2005). The pharmacology of PAR1 is well developed, with widely available subunit selective agonists, potent and selective antagonists, and viable PAR1−/− mice. Figure 1 summarizes intracellular Ca^{2+} signalling in response to PAR1 activation in cultured astrocytes, with virtually all wild-type mouse astrocytes showing a robust increase in fluorescence of the Ca^{2+} sensitive dye Fura-2 in responses to the application of 30 nM thrombin (Fig. 1*A*, left panels) and 30 μM of the selective PAR1-activating peptide TFLLR (at least 3-fold EC_{50}; Hollenberg *et al.* 1997). Both the agonist peptide that mimics the cleaved N-terminal (TFLLR, 30 μM) and the serine protease thrombin (30 nM) selectively activate PAR1, being without effect in PAR1−/− mice ($n = 3$ for TFLLR, $n = 5$ for thrombin, $P < 0.05$ paired t test, Fig. 1*A*, right panels, and Fig. 1*B* and *D*). ATP served as a positive control in PAR1−/− mice. In addition, 1 μM of the PAR1 antagonist BMS200261 (Bernatowicz *et al.* 1996; Kawabata *et al.* 1999) can selectively and reversibly block astrocytic PAR1 activation by either 30 μM TFLLR (Fig. 1*C*; $n = 4$ experiments; $P < 0.01$) or 30 nM thrombin (Fig. 1*E*; $n = 4$ experiments; $P < 0.01$). These data suggest that a modest concentration of thrombin (30 nM) was relatively selective for PAR1 activation, since removal or block of PAR1 eliminated the intracellular Ca^{2+} response in cultured astrocytes. These results are consistent with a number of previous reports in the literature suggesting that thrombin stimulates Ca^{2+} mobilization in neurones and glia (Smith-Swintosky *et al.* 1995; Yang *et al.* 1997; Smirnova *et al.* 1998; Wang *et al.* 2002*a*,*b*; Suo *et al.* 2002; Sorensen *et al.* 2003; Junge *et al.* 2004; Nicole *et al.* 2005). The TFLLR-induced astrocytic Ca^{2+} responses persisted in the absence of external Ca^{2+} (Fig. 1*F*; $n = 4$, $P > 0.05$) and were blocked by pretreatment with 1 μM thapsigargin (Fig. 1*F*; $n = 4$, $P < 0.05$). Treatment with the cell-permeant Ca^{2+} chelator BAPTA-AM (50 μM) eliminated the PAR1-evoked fluorescence response of Ca^{2+} sensitive dyes (Fig. 1*G*; $n = 4$, $P < 0.05$). Finally, 2 μM of the phospholipase C inhibitor U73122 blocked TFLLR-induced increases in Ca^{2+} responses (Fig. 1*G*; $n = 3$, $P < 0.05$), suggesting that PAR1 stimulates Ca^{2+} release from inositol triphosphate-sensitive stores in astrocytes.

to the positive control 10 μM ATP. *E*, 30 nM thrombin has no significant effect on wild-type astrocytes pretreated with 1 μM of the PAR1 antagonist BMS 200261. TFLLR applied before and after thrombin's application served as a positive control. *F*, TFLLR (30 μM) increased intracellular Ca^{2+} concentration in the nominal absence of extracellular Ca^{2+}; pre-exposure to 1 μM thapsigargin blocked the subsequent response to TFLLR application. *G*, treatment of mouse astrocytes with 50 μM BAPTA-AM for 30 min after an initial TFLLR application blocked the Ca^{2+} response to subsequent TFLLR application. Treatment of the PLC inhibitor U-73122 (2 μM) for 10 min similarly blocked the effects of TFLLR.

Activation of glial PAR1 in brain slices elevates intracellular Ca^{2+}

To test the hypothesis that PAR1 signalling pathways similar to those described in culture occur in brain tissue, we studied the effects of PAR1 activation in neurones and glial cells in acutely prepared rat brain slices. Consistent with the *in situ* hybridization and immunohistochemistry (Weinstein *et al.* 1995; Striggow *et al.* 2001; Wang *et al.* 2002*b*; Junge *et al.* 2004), we found robust TFLLR-evoked increases in fluorescence in CA1 stratum radiatum glial cells recorded using whole cell patch methods and pipettes loaded with Ca^{2+}-sensitive fluorescent dyes (Fig. 2*A*–*D*; $n = 5$). Glial cells were identified by their small somatic size and distinct morphology (Fig. 2*A*, left panel), negative resting potential, lack of voltage-dependent currents, and low input resistance (Fig. 2*A*, right panel). CA1 pyramidal cells were identified by their location in stratum pyramidale, their morphology (Fig. 2*E*, left panel) and the presence of action potentials upon a series of injected current steps (Fig. 2*E*, right panel). We could not detect any significant increase in somatic fluorescence of Ca^{2+}-sensitive dyes to application of thrombin (30 nM) or TFLLR (30 μM) to CA1 pyramidal neurones in hippocampal slices (Fig. 2*E* and *F*; $n = 17$). Either the broad spectrum metabotropic glutamate receptor (mGluR) agonist *trans*-ACPD (100 μM) or the group I mGluR agonist (*S*)-3,5-dihydroxyphenylglycine (30 μM) served as a positive control; both agonists evoked strong increases in somatic neuronal Ca^{2+} fluorescence in all cells tested.

We additionally performed imaging of Ca^{2+} sensitive dye Fura-2-AM loaded into acutely dissociated cells from the CA1 region dissected from hippocampal slices to further screen for TFLLR responsive cells (see Methods). We found that 24 of 25 TFLLR-responsive cells were unresponsive to NMDA, suggesting they were

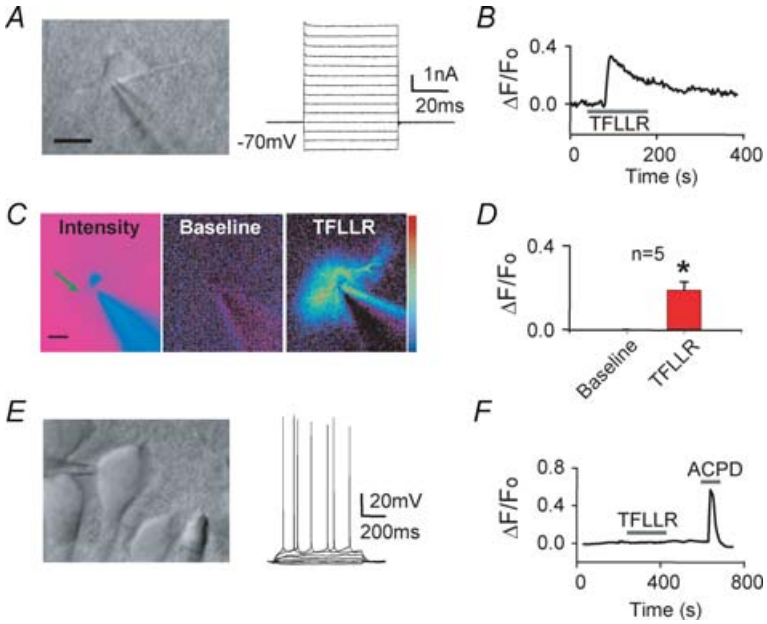

Figure 2. TFLLR increases intracellular Ca^{2+} in glial cells but not in CA1 pyramidal cells in hippocampal slices

A, DIC image of a glial cell (left panel) patched with 100 μM Oregon Green 488 BAPTA-2 included in the patch pipette (16 MΩ input resistance; $V_H = -70$ mV; $V_M = -76$ mV). Voltage steps of 10 mV were applied to this cell under voltage clamp (right panel), and revealed a linear current–voltage relationship with no activation of time-dependent currents. Calibration bar is 10 μm. *B*, changes in fluorescence intensity in the glial cell in *A* are shown during application of 30 μM TFLLR. *C*, fluorescence intensity in a glial cell (left, Intensity), also shown as fluorescent change as a $\Delta F/F_0$ (as in *B*) before (centre, Baseline) and after 30 μM TFLLR application (right, *TFLLR*). The baseline image is generated by taking the ratio of $(F - F_0)/F_0$, where F_0 is the first intensity image. During TFLLR application the ratio increased significantly in the soma as well as the processes. The colour scale on the right shows the pseudocolour coding of ratio values ranging from 0 (bottom) to 0.4 (top). *D*, the average changes in fluorescence are shown (± S.E.M.). The arrow in the left panel of *C* shows where the changes in fluorescence are monitored. $^*P < 0.05$, paired *t* test. *E*, DIC image of a CA1 pyramidal neurone (left panel), patched with 100 μM Fluo-3 included in the patch pipette ($V_M = -62$ mV left panel). Current injection of 10 pA steps under applied current clamp; membrane voltage changes and action potentials in this neurone are shown in the right panel. *F*, changes in somatic fluorescent intensity in dye-loaded CA1 neurones during application of 30 μM TFLLR and 100 μM *trans*-ACPD, a broad spectrum metabotropic glutamate receptor agonist used as a positive control.

non-neuronal (data not shown). This is in striking contrast to only 1 of 24 NMDA-responsive neurones that showed a response to PAR1 activation. These data together suggest that functional coupling of PAR1 to Gαq/11-mediated Ca^{2+} signalling is largely restricted to glial cells in the CA1 region of hippocampus. The ∼4% of acutely dissociated neurones from the CA1 region that respond to PAR1 activation by increasing intracellular Ca^{2+} is consistent with our data in slice recordings (Fig. 2) as well as with other reports in the literature (e.g. Yang *et al.* 1997), but is lower than our previous estimate of ∼40% of thrombin responsive neurones in cultures prepared from the entire hippocampal formation plus dentate gyrus (13% respond to thrombin + inhibitor, 54% respond to 30 nM thrombin; Gingrich *et al.* 2000). This discrepancy likely reflects higher PAR1 expression in dentate granule neurones than in CA1 neurones (Weinstein *et al.* 1995).

Activation of astrocytic PAR1 stimulates Ca^{2+}-dependent release of glutamate

Astrocytes have long been known to be involved in glutamate homeostasis, taking up synaptically released glutamate via several molecularly distinct transporters (Anderson & Swanson, 2000; Danbolt, 2001). However, astrocytes or NG2 glial cells can also respond to synaptically released glutamate through activation of AMPA receptors (Dzubay & Jahr, 1999; Bergles *et al.* 1999, 2000) or group I mGluR (Wang *et al.* 2006), can propagate Ca^{2+} waves (Schipke *et al.* 2002), and are extensively coupled (D'Ambrosio *et al.* 1998; reviewed by Haydon, 2001; Nedergaard *et al.* 2003). Under circumstances where intracellular Ca^{2+} is elevated, astrocytes can release glutamate into the extracellular space (Parpura *et al.* 1994; Nedergaard, 1994) by a range of mechanisms including regulated exocytosis (Bezzi *et al.* 1998; Araque *et al.* 2000; Fellin *et al.* 2004) as well as by channel-related mechanisms (Kimelberg *et al.* 1990; Longuemare & Swanson, 1995; Raiteri *et al.* 2001; Duan *et al.* 2003; Ye *et al.* 2003). Since PAR1 activation in astrocytes increases the intracellular Ca^{2+} concentration, we examined whether activation of PAR1 by TFLLR can stimulate the release of glutamate from cultured astrocytes. As shown in Fig. 3, release of glutamate, as measured by the efflux of radiotracer from [^{3}H]glutamate loaded cultures (Duan *et al.* 2003), was significantly increased upon TFLLR application by $56 \pm 9\%$ compared to the control (Fig. 3; $n = 14$). This increase in glutamate release was not observed in astrocyte cultures prepared from PAR1−/− mice ($n = 4$), and was blocked by BAPTA-AM treatment ($n = 3$), indicating the PAR1 selectivity and Ca^{2+} dependence of glutamate release. Glutamate release was measured in both the absence and the presence of a maximally effective concentration of the glutamate uptake blocker *trans*-PDC (50 μM, $IC_{50} = 4$–8 μM; Mitrovic & Johnston, 1994; Esslinger *et al.* 2002) (data not shown) and was indistinguishable, suggesting that release did not reflect reversal of the glutamate uptake pump. The level of *trans*-PDC utilized here was below the threshold level proposed to stimulate heteroexchange (0.2 mM; Volterra *et al.* 1996; Bezzi *et al.* 1998).

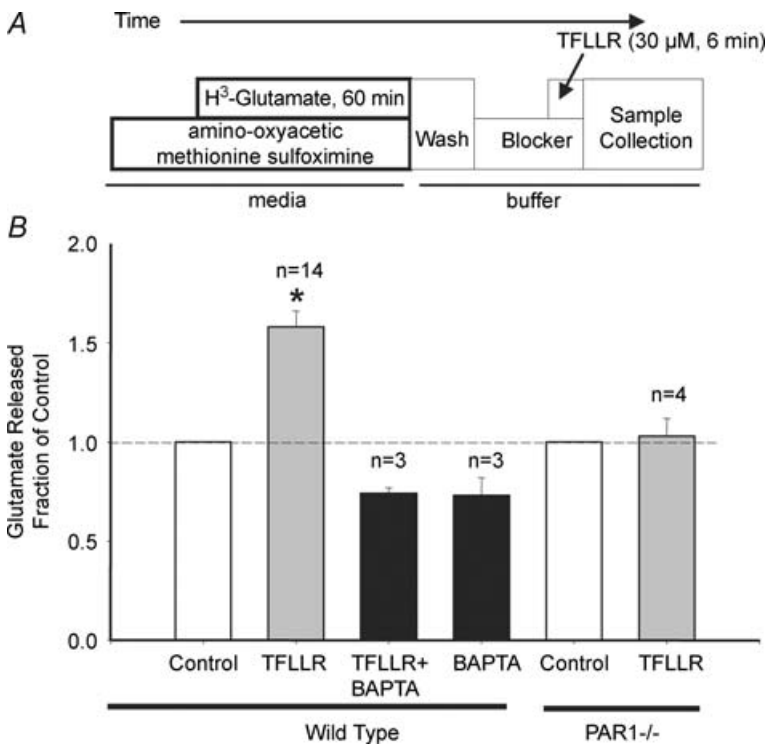

Figure 3. PAR1 activation stimulates Ca^{2+}-dependent release of glutamate in astrocytes
A, schematic diagram summarizing the experimental protocol for assaying glutamate release from cultured astrocytes. To inhibit the conversion of glutamate to glutamine and other metabolites, amino-oxyacetic acid (1 mM) and methionine sulfoximine (0.5 mM) were preincubated for 30 min and included throughout the loading of [^{3}H]glutamate. Cells were washed with external solution and TFLLR and other drugs were subsequently added for 6 min. In some experiments, the external solution was supplemented with 50 μM *trans*-PDC to block the glutamate transporter, a level well below that known to stimulate heteroexchange (Volterra *et al.* 1996; Bezzi *et al.* 1998). The thick boxes represent cells in culture medium; the thin boxes represent cells in external solution. *B*, bar graph showing that TFLLR induced a significant increase in glutamate release that was blocked by 30 min treatment of 50 μM BAPTA-AM. The increase in glutamate release by TFLLR was absent in PAR1−/− astrocytes. Numbers on top of each bar indicate number of 6-well plates. $^*P < 0.05$, 1-factor ANOVA with Dunnett's test for wild-type, unpaired *t* test for PAR1−/−.

In order to evaluate PAR1-stimulated glutamate release in real time, we developed a 'sniffer-patch' detection system in which HEK 293 cells transfected with the non-desensitizing GluR1 mutant L497Y (Stern-Bach *et al.* 1998) were used as a biosensor of glutamate release from cultured cortical astrocytes (in Fig. 4*A*). GluR1(L497Y) responds to glutamate with a sustained current that will temporally follow the glutamate concentration. Thus, this technique provides millisecond time resolution for the detection of micromolar levels of glutamate released from astrocytes. We plated GluR1(L497Y)-transfected HEK cells directly onto an astrocyte monolayer, and subsequently recorded the whole cell HEK current response under voltage clamp during brief 0.2 s application of the PAR1 activator TFLLR (500 μM), ATP (300 μM), or bradykinin (180 μM) from a pressurized pipette (Fig. 4*A* and *B*). As expected, simultaneous electrophysiological and Ca^{2+} sensitive dye Fura-2-AM recordings revealed that TFLLR, ATP and bradykinin all increased astrocytic intracellular Ca^{2+} and elicited an inward current in HEK cells expressing GluR1(L497Y) (Fig. 4*B*). Only HEK cells expressing GluR1(L497Y) responded to pressure application of TFLLR, bradykinin, or ATP with an inward current, which was blocked by 10 μM of the AMPA receptor antagonist CNQX (Fig. 4*C* and *D*; $n = 7$). No TFLLR-induced HEK current responses could be detected when GluR1(L497Y)-transfected HEK cells were cocultured on an astrocyte feeder layer derived from PAR1−/− animals (Fig. 4*D*; $n = 6$). Simultaneous imaging of Ca^{2+}-sensitive fluorescent dyes confirmed that TFLLR did not alter PAR1−/− astrocytic intracellular Ca^{2+} but did increase HEK cell intracellular Ca^{2+}, as expected given endogenous expression of PAR1 in HEK cells (data not shown). These control experiments were performed on the same day as TFLLR stimulation of HEK cells on wild-type astrocytes, and confirm that PAR1 activators had no direct effect on GluR1(L497Y) currents in HEK cells. Evaluation of the HEK GluR1(L497Y)-mediated current response after the experiment to a maximally effective concentration of glutamate (1 mM) suggested that the TFLLR-stimulated release of glutamate evoked a response that was on average 10 ± 2.6% of the maximal achievable response (Fig. 4*E* and *G*; $n = 13$). Because GluR1(L497Y) receptors give non-desensitizing responses to glutamate in HEK cells with an EC_{50} value of 6.1 μM (Fig. 4*E*; Hill slope 1.3), we can directly calculate the concentration time course of glutamate released using the equation

$$\text{Concentration}\,(t) = \text{EC}_{50}\,[\text{response}(t)/(100 - \text{response}(t))]^{(1/n)}$$

where response(t) is the response amplitude expressed as a percentage of the maximum achievable response and n is the Hill slope. Using this expression, we estimate that glutamate reaches a peak value on average of 1.1 μM, and decays with an approximately exponential time course (Fig. 4*F* and *G*), which in this system is a complex reflection of diffusion, uptake, and intracellular astrocytic Ca^{2+} dynamics. Bradykinin and ATP induce glutamate concentrations approaching 3.9 and 5.9 μM, respectively. These data (Fig. 4*G*) strongly suggest that activation of astrocytic PAR1 can stimulate glutamate release from astrocytes by a Ca^{2+}-dependent mechanism, and that levels of extracellular glutamate are sufficient to activate glutamate receptors.

We performed two experiments using our sniffer-patch detection system to verify that the astrocytic release of glutamate we observed did not reflect a culture artifact. First, cultures were prepared in the absence of glutamine, which should prevent artifactual elevation of intracellular glutamate concentration that might have skewed levels of glutamate release we observed (Bak *et al.* 2006). However, TFLLR application evoked an identical CNQX-sensitive response in GluR1(L497Y) transfected HEK cells when astrocytes were cultured in glutamine-free medium, suggesting that TFLLR-induced glutamate release was not solely the result of potentially high intracellular glutamate that might arise in glutamine-supplemented culture medium (online Supplementary Fig. 2). TFLLR induced a current response that was 9.7 ± 1.3% ($n = 4$) of the maximal response from astrocytes cultured in the absence of glutamine, which was not significantly different from 10 ± 2.6% ($n = 13$; $P > 0.05$) in the presence of glutamine. In addition, we also acutely dissociated cells from CA1 region of hippocampal slices prepared from transgenic mice expressing GFP under control of the GFAP promoter (Brenner *et al.* 1994). This allowed us to unambiguously identify isolated hippocampal astrocytes which had not been subject to tissue culture. Cells were dissociated directly onto GluR1(L497Y)-transfected HEK cells. We subsequently identified GFP-expressing astrocytes that came to rest adjacent to a GluR1(L497Y)-transfected HEK cell (Fig. 5*A*), and used patch clamp recordings from the GluR1(L497Y)-transfected HEK cell to detect glutamate release from the astrocyte. We only studied GFP-positive astrocytes with low resting levels of intracellular Ca^{2+}, which are invariably healthy cells with normal electrical properties. Figure 5 shows the results from a representative experiment in which brief application of the selective PAR1 activator TFLLR from a pressurized pipette evoked a response in a nearby GluR1(L497Y)-transfected HEK cell. Similar results were found in 4 cells (1.46 ± 0.54 μM; $n = 4$), which confirm that glutamate release can occur from astrocytes in slices.

Because PAR1 activators induce little or no intracellular Ca^{2+} signalling in CA1 pyramidal cells or acutely dissociated CA1 neurones, we predicted that PAR1 activators will not induce glutamate release from

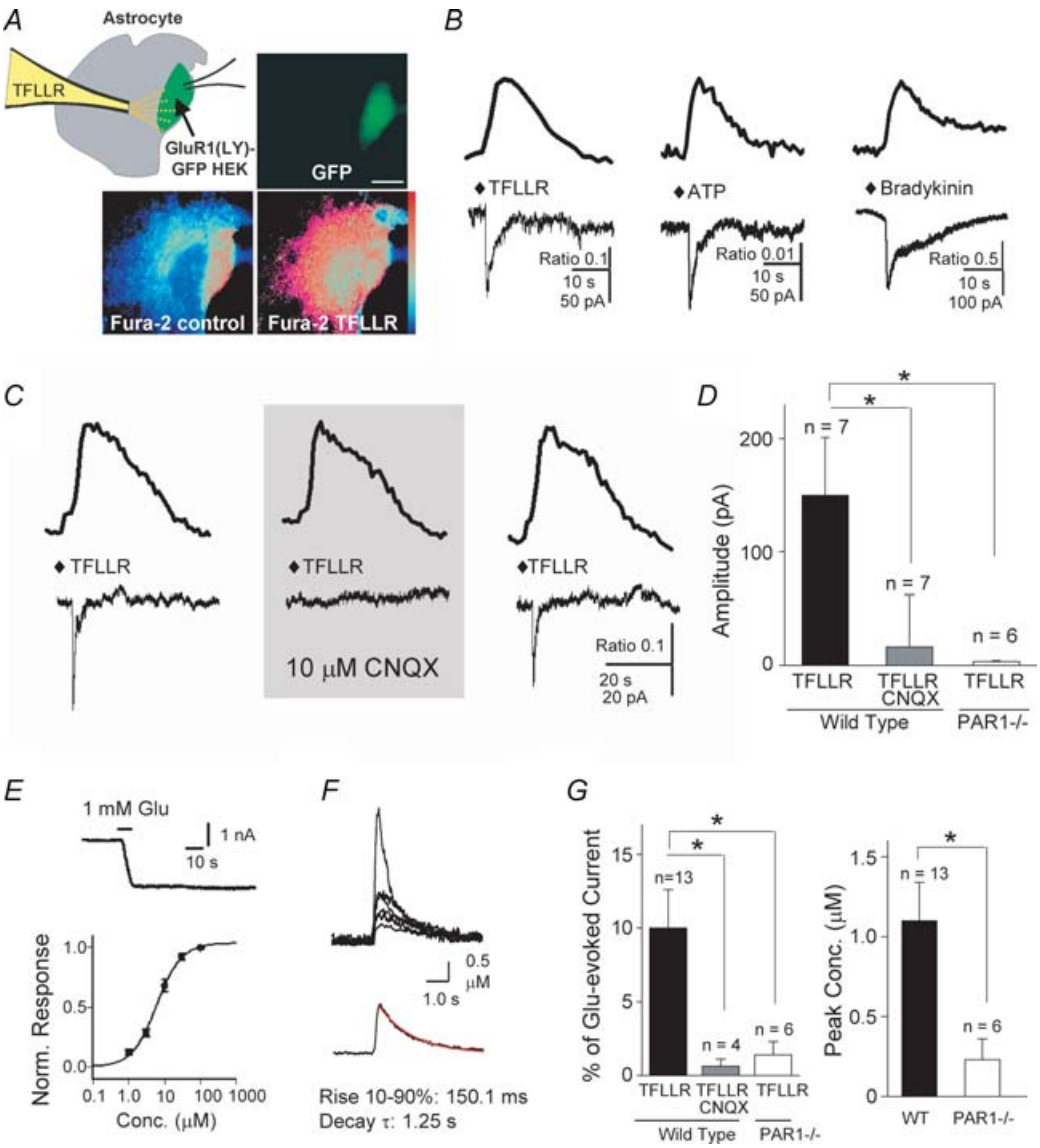

Figure 4. Use of GluR1(L497Y) transfected HEK cells as biosensors for astrocytic glutamate release
A, schematic diagram illustrating experimental setup is shown together with GFP fluorescent image of astrocyte–GluR1(L497Y)–GFP transfected HEK cell coculture (upper left panel). The lower panel shows the ratio image (510 nm emission; 340 nm/380 nm excitation) of Fura-2-AM loaded cocultures before and after brief (< 1 s) pressure-applied TFLLR (500 μM in pipette). Calibration bar is 20 μm. *B*, quantification of the fluorescence increase in response to brief (< 1 s) pressure application of 500 μM TFLLR, 300 μM ATP and 180 μM bradykinin from a pipette in a wild-type astrocyte (upper trace) recorded together with the inward current induced in an adjacent GluR1(L497Y)-transfected HEK cell (lower trace). *C*, CNQX reversibly inhibits TFLLR-evoked inward current in GluR1(L497Y) in a representative transfected HEK cell. The upper trace is Fura-2 fluorescence ratio, the lower trace is inward current. *D*, summary response in GluR1(L497Y) transfected HEK cells to TFLLR application to astrocytes shown as peak current in wild-type and PAR1−/− astrocyte cultures. CNQX significantly reduced the response of GluR1(L497Y)-transfected HEK cells to TFLLR application ($n = 7$; $P < 0.05$, 1-factor ANOVA). There is virtually no detectable current response recorded from GluR1(L497Y)-transfected HEK cells cocultured with PAR1−/− astrocytes in response to pressure application of TFLLR (3.4 ± 0.8 pA, $n = 6$, $P < 0.05$, 1-factor ANOVA, compared with wild-type response amplitude). *E*, the current response to pressure application of TFLLR was converted to concentration using the dose–response relationship and maximal current response of the GluR1(L497Y) transfected HEK cell as described in the Methods. EC_{50} value for glutamate activation of GluR1(L497Y) in transfected HEK cells was 6.1 μM (Hill slope 1.3). *F*, concentration responses from 7 cells are shown superimposed (upper panel) and below as an average (lower panel). *G*, summary response in GluR1(L497Y) transfected HEK cells to TFLLR application to astrocytes shown as percentage of the maximal response (TFLLR on WT: 10 ± 2.6%; TFLLR + CNQX on WT: 0.64 ± 0.47%; TFLLR on PAR1−/−: 1.4 ± 0.9%, $^*P < 0.05$, 1-factor ANOVA), and concentration (WT: 1.1 ± 0.24 μM; PAR1−/−: 0.23 ± 0.13 μM, $^*P < 0.05$, unpaired *t* test) in wild-type and PAR1−/− astrocyte cultures.

neurones. Figure 6*A* shows the ability of our GluR1 (L497Y)-transfected HEK coculture system to detect CNQX-sensitive glutamate release from neurones in response to hyperosmotic solutions (530 mosmol l^{-1}, $n = 6$), which stimulate vesicular release of glutamate from cultured central neurones (e.g. Bekkers & Stevens, 1989, Bekkers & Stevens, 1995). By contrast, brief application of TFLLR caused no detectable glutamate-induced current in GluR1(L497Y)-transfected HEK cells adjacent to neurones (Fig. 6*B*; $n = 3$). As a positive control for TFLLR activation of PAR1, we could readily record on the same day glutamate responses to activation of PAR1 in astrocytes (Fig. 6*C*; $n = 4$). We subsequently examined the effects of PAR1 activators on NMDA receptor responses in neurones as well as the effect of activation of endogenous PAR1 in HEK cells on recombinant NR1/NR2A receptors. We could detect no change in neuronal (data not shown) or recombinant NMDA receptor response properties before and after thrombin treatment (Supplementary Fig. 3). These data suggest that PAR1 signalling in mammalian cells does not directly lead to post-translational modification of the receptor, in contrast to previous conclusions from studies of PAR1 and NMDA receptors coexpressed in *Xenopus laevis* oocytes (Gingrich *et al.* 2000). Because we can replicate potentiation in the oocyte but cannot observe NMDA receptor potentiation in mammalian cells, we conclude that the intracellular signalling pathways linked to PAR1 in these two cells must differ. Other investigators have also noted differences in post-translational modification of recombinant NMDA receptors expressed in mammalian cells *versus* oocytes (Xiong *et al.* 1998).

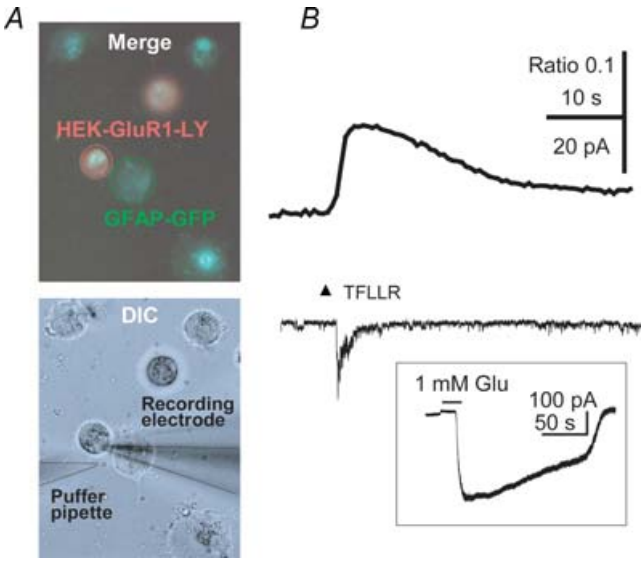

Figure 5. TFLLR-evoked glutamate release from acutely dissociated CA1 astrocytes
A, merged images of acutely dissociated GFAP–GFP labelled astrocytes (green) plated onto GluR1(L497Y) transfected HEK cells (red; upper panel). The lower panel shows a DIC image of the same coculture as above with the recording electrode and pressurized agonist-filled pipette outlined (dotted lines). *B*, representative traces of Fura-2 fluorescence increase in GFAP–GFP labelled astrocyte (upper trace) recorded together with the inward current from GluR1(L497Y) transfected HEK cell (lower trace) in response to brief (< 1 s) application of TFLLR (500 μM in pipette). Inset is the response to 10 s application of a maximally effective concentration of glutamate (1 mM) on the same cell.

Astrocytic PAR1-mediated glutamate release can activate neuronal NMDA receptors in culture

To test whether astrocyte-released extracellular glutamate rises to sufficient levels to activate NMDA receptors on neuronal dendrites, we modified the coculture system described above, replacing GluR1(L497Y)-transfected HEK cells with cortical neurones derived from PAR1−/− animals growing on top of a wild-type astrocyte monolayer that was determined to be > 95% GFAP positive cells (Nicole *et al.* 2005). We could not detect any NMDA responsive Fura-2 loaded cells in our wild-type astrocyte monolayers before plating of neurones from PAR1−/− mice (data not shown). These data show that all neurones in subsequent cocultures were derived from PAR1−/− animals and did not arise as contaminating wild-type neurones from preparation of the astrocyte monolayer. Use of PAR1−/− neurones allowed us to evaluate NMDA receptor responses to TFLLR-induced glutamate release without the confounding variable of potential intraneuronal PAR1 activation. An individual neurone was dye-loaded through a patch electrode containing 100 μM of the Ca^{2+} indicator dye Oregon Green 488 BAPTA-2 ($K_d = 580$ nM) for 1–2 min after breakthrough, and the patch electrode was subsequently withdrawn from the cell. After a 20 min recovery, the bath perfusion was stopped and TFLLR was applied by brief (< 1 s) pressure ejection onto the astrocyte hosting the dye-loaded neurone in a static bath condition. Changes in fluorescence were monitored in a number of dendritic processes (schematized in Fig. 7*A* and *B*). As summarized in Fig. 7*C*, TFLLR-induced increases in Oregon Green BAPTA-2 fluorescence could be observed in the dendrites, and this increase was blocked by the competitive NMDA receptor antagonist, D-2-amino-5-phosphono-valeric acid (APV; 50 μM). Complimentary experiments were performed with the same culture system in which PAR1−/− neurones were recorded under voltage clamp during activation of astrocytic PAR1 (Fig. 7*D*). We observed a clear inward current (peak amplitude: 51 ± 8.8 pA; $n = 6$) during activation of astrocytic PAR1 by bath application of 30 μM TFLLR. This TFLLR-evoked current was blocked by 50 μM APV (peak amplitude: 2.5 ± 0.3 pA, $n = 3$), suggesting it reflects NMDA receptor activation. Together these two results strongly suggest that the glutamate released by the

astrocytes onto neurones in culture reach sufficient levels to activate NMDA receptors.

Astrocytic PAR1 activation depolarizes neurones in slices

To determine if PAR1-mediated glutamate release can occur in slices, we obtained whole cell patch recordings under voltage clamp from CA1 pyramidal cells during application of the PAR1 selective peptide agonist TFLLR (30 μM) or thrombin (30 nM). After establishing a whole cell recording, we subsequently bathed slices in ACSF containing reduced Mg^{2+} (5 μM) supplemented with 0.5 μM tetrodotoxin for 15 min to allow measurement of the NMDA receptor current response. The stable baseline we obtained suggests that this duration of low Mg^{2+} ACSF was sufficient to reduce extracellular Mg^{2+} to a stable level. We observed a clear inward current in response to thrombin (Fig. 8*A* and *B*; $n = 8$) or TFLLR (Fig. 8*B*; $n = 7$), which was APV-sensitive for both PAR1 activators. We also observed a clear and significant increase in current fluctuations during the TFLLR or thrombin application in the presence of low external Mg^{2+}. We quantified the noise increase by measuring the current variance in stretches of recordings with no spontaneous mEPSCs. Application of 30 μM TFLLR or 30 nM thrombin significantly increased the current variance, and this increase was reversed by the competitive NMDA receptor antagonist D-APV (50 μM; Fig. 8*C* and *D*). This finding, coupled with the lack of any detectable PAR1 signalling in CA1 pyramidal cells (Fig. 2)

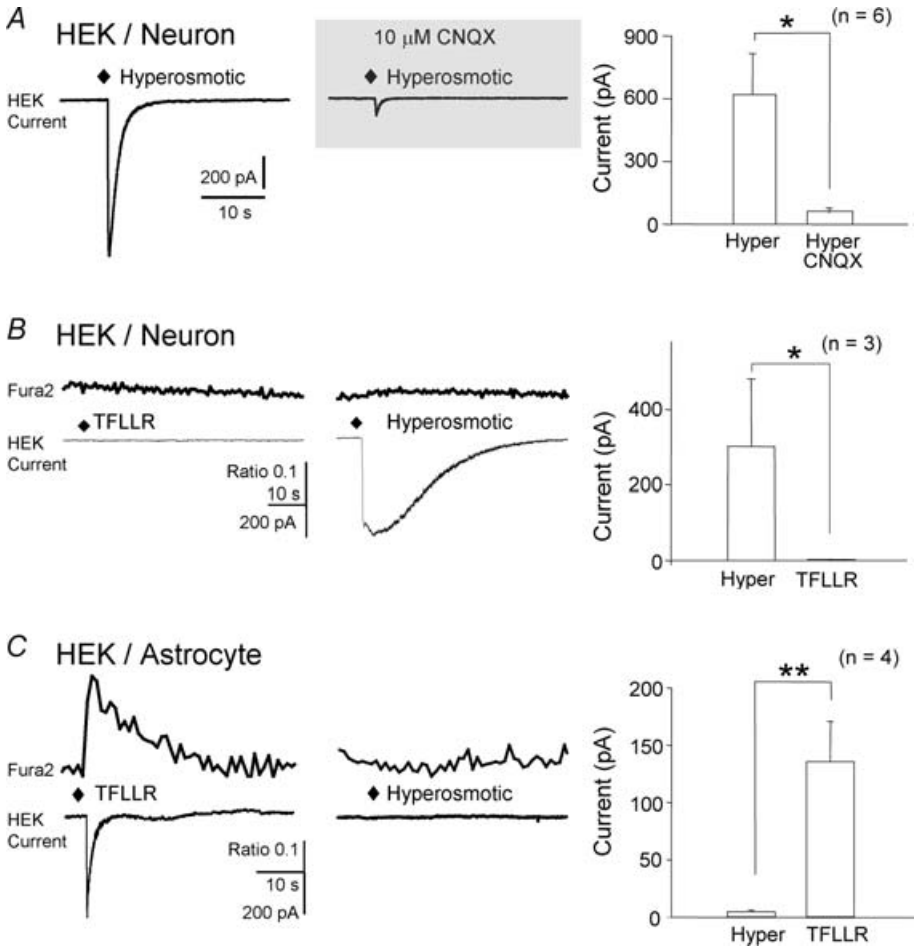

Figure 6. PAR1 activation releases glutamate from cultured astrocytes but not cultured neurones
A, GluR1(L497Y)-transfected HEK cell can detect neuronal glutamate release by hyperosmotic solution (530 mosmol l^{-1}). The detection is abolished by the treatment of 10 μM CNQX. Right panel is the summary of the current amplitude changes; $^*P < 0.05$; paired *t* test ($n = 6$). *B*, a HEK cell expressing GluR1(L497Y) adjacent to a cultured neurone shows virtually no response to application of 30 μM TFLLR onto the neurone (3.0 $\pm$ 0.1 pA, $n = 3$). By contrast, the same cell can detect the neuronal glutamate released upon the treatment with hyperosmotic solution (301.6 $\pm$ 179.3 pA, $n = 3$, $^*P < 0.05$; paired *t* test). *C*, HEK cell expressing GluR1(L497Y) can detect the glutamate release from astrocytes during application of TFLLR (136 $\pm$ 35 pA, $n = 4$), yet shows virtually no response to application of hyperosmotic solution (4.8 $\pm$ 1.4 pA, $n = 4$, $^{**}P < 0.01$; unpaired *t* test).

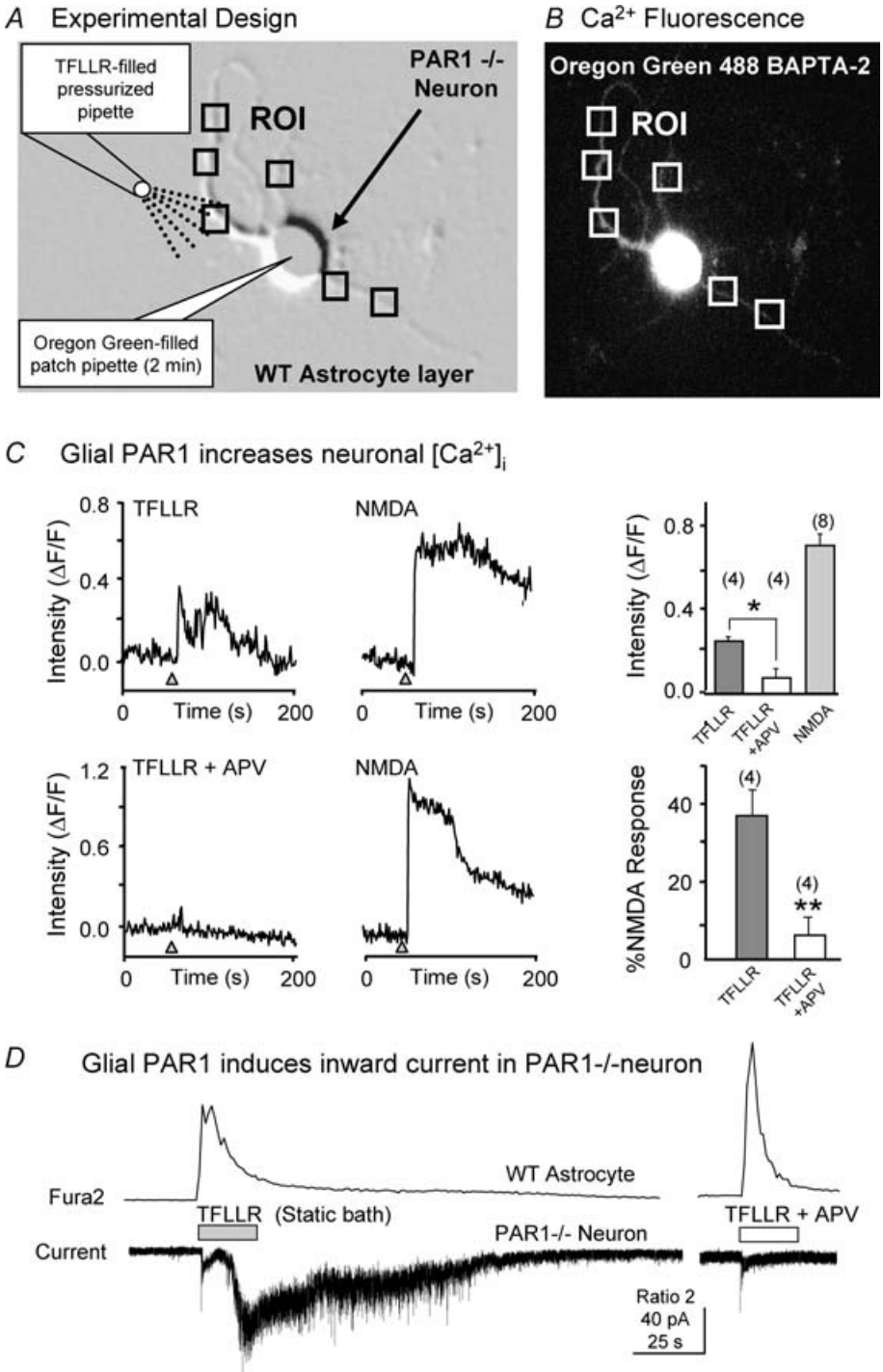

Figure 7. PAR1 activation in astrocytes activates NMDA receptors in neighbouring neurones
A, photomicrograph of a PAR1−/− cortical neurone that was loaded with 300 μM Oregon Green BAPTA-2 for 2 min through a patch pipette after breaking the gigaohm seal. Several regions (boxes) at distal dendrites were imaged while 300 μM TFLLR was pressure applied briefly (1 s) from a pipette to surrounding wild-type astrocytes. TFLLR application increased the intraneuronal Ca^{2+} concentration throughout the dendrites. *B*, fluorescence image of the same PAR1−/− neurone, loaded with Oregon Green 488 BAPTA-2, 450–490 nm excitation, 520 nm emission). *C*, average fluorescence intensity response from 6 regions of interest on dendrites shown during brief TFLLR pressure application (marked by triangle; upper left traces). TFLLR applied in the presence of 100 μM DL-APV had no effect on intracellular Ca^{2+} in dendrites (lower left traces). NMDA at 50 μM caused a saturating response in the same regions of interest. The peak fluorescence intensity change was obtained in response to TFLLR for each neurone, and mean values are compared for TFLLR, TFLLR in the presence of APV, and NMDA as a bar graph (upper right

and the lack of glutamate release from neurones (Fig. 6), strongly suggests that activation of astrocytic PAR1 stimulates release of glutamate that can in turn activate neuronal NMDA receptors in brain slices.

In order to determine whether PAR1-evoked glutamate release was sufficient to depolarize neurones under normal conditions, we evaluated the effect of 30 nM thrombin on membrane potential of CA1 pyramidal cells in hippocampal slices bathed in normal ACSF (nominal 1.5 mM Mg^{2+}). We found a significant membrane depolarization (5.7 ± 0.9 mV, range 0–15 mV, $n = 22$, $P < 0.05$, paired t test; Fig. 8*E*, right panel) in current clamp recording from CA1 pyramidal neurones in hippocampal slices. Additional current clamp recordings showed that application of APV (100 μM) significantly reduced the thrombin-induced depolarization. APV itself has no significant effect on the resting membrane potential of CA1 neurones (0.4 ± 0.7 mV; $n = 4$; $P = 0.32$; paired t test); the residual depolarization in APV was not significantly different from 0 mV ($P > 0.05$; 1-factor repeated measures ANOVA with Dunnett's test). To verify that the APV-sensitive PAR1-mediated depolarization persisted in conditions of vigorous glutamate uptake, this experiment was repeated in slices held at 34°C. Identical results were found in that 30 nM thrombin induced a significant membrane depolarization that was significantly reduced by APV ($n = 12$; Fig. 8*F*). The APV sensitivity of the thrombin effect strongly supports the idea that PAR1-induced glutamate release from astrocytes depolarizes neurones through activation of NMDA receptors.

Astrocytic PAR1-mediated glutamate release enhances synaptic NMDA receptor currents in slices

Because PAR1 activation causes both depolarization (data above) as well as voltage- and Mg^{2+}-dependent potentiation of NMDA receptors (Gingrich *et al.* 2000), we reasoned that PAR1-mediated depolarization of distal dendrites under poor voltage control might account for NMDA receptor potentiation previously observed through partial relief of Mg^{2+} block (Gingrich *et al.* 2000). To test the idea that PAR1-stimulated glutamate release can depolarize distal dendrites in a manner that reduces Mg^{2+} block of synaptic NMDA receptors, we examined the current–voltage (I–V) relationship for synaptically evoked excitatory postsynaptic currents (EPSCs) following PAR1 activation (Fig. 9*A* and *B*). EPSCs were evoked by electrical stimulation of Schaffer collateral axons in the CA1 stratum radiatum, and recorded from CA1 pyramidal neurones under voltage clamp. External Mg^{2+} was reduced to 200 μM to allow measurement of NMDA receptor-mediated currents before PAR1 activation at hyperpolarized potentials where Mg^{2+} block is profound. All experiments were performed in the presence of 5 μM glycine, 20 μM CNQX and 20 μM bicuculline to isolate the NMDA receptor component of the EPSCs, which decayed with a characteristically slow exponential time course (mean τ_{decay} 96 ms; $n = 6$) that could be blocked by 100 μM APV (Fig. 9*C*). Cells were held under voltage clamp at −60 mV, and the membrane potential stepped through six levels (+25 mV steps) every 30 s; I–V curves were collected every 5 min. After three baseline I–V curves were recorded, perfusion of the slice was switched to a reservoir containing either the same low Mg^{2+} artificial cerebrospinal fluid (ACSF) or low Mg^{2+} ACSF supplemented with 30 nM thrombin. The shape of the current–voltage relationship did not change in low Mg^{2+} ACSF-perfused control cells indicating no mechanical or perfusion artifact occurred with the solution switch (Fig. 9*A*). However, the NMDA receptor I–V curve was altered in thrombin-treated cells (Fig. 9*B*), with EPSCs showing significantly less Mg^{2+} block at a holding potential of −60 mV compared to control cells (Fig. 9*D* and *E*). These results suggest that the PAR1 potentiation of NMDA receptor is most prominent at −60 mV, consistent with the idea that PAR1 activation causes a partial relief of Mg^{2+} blockade at this potential that is secondary to distal dendrite depolarization that cannot be controlled under voltage clamp.

To investigate the effects of PAR1 activation on synaptic NMDA receptors in normal concentrations of Mg^{2+} (1.5 mM), we recorded spontaneous miniature excitatory postsynaptic currents (mEPSCs) at −60 mV in the presence of 0.5 μM TTX to look for changes in the amplitude and decay kinetics of individual synaptic currents. As shown in Fig. 10*A*, glutamatergic mEPSCs (frequency 0.1–0.5 Hz) recorded in the presence of 10 μM bicuculline and 1.5 mM extracellular Mg^{2+} showed the characteristic rapid rise and decay times, suggesting they arise primarily from AMPA receptor activation, with NMDA receptors subjected to strong voltage-dependent block by Mg^{2+}. mEPSC rise time displayed a skewed distribution, which we interpret to reflect different

panel). There was a significantly larger Ca^{2+} increase with TFLLR than with TFLLR in the presence of APV, $^{*}P < 0.01$, paired t test. Numbers in parentheses indicate the number of neurones tested. Data from the same experiment were also normalized to the response to NMDA application (lower right panel); $^{**}P < 0.05$, paired t test. *D*, activation of astrocytic PAR1 induces APV-sensitive inward current in PAR1−/− neurones. TFLLR at 30 μM (bath application) increased intracellular Ca^{2+} level of wild-type astrocytes and simultaneously induced an inward current in adjacent PAR1−/− neurone (51 ± 8.8 pA, $n = 6$). The current was abolished in the presence of 100 μM DL-APV (right panel).

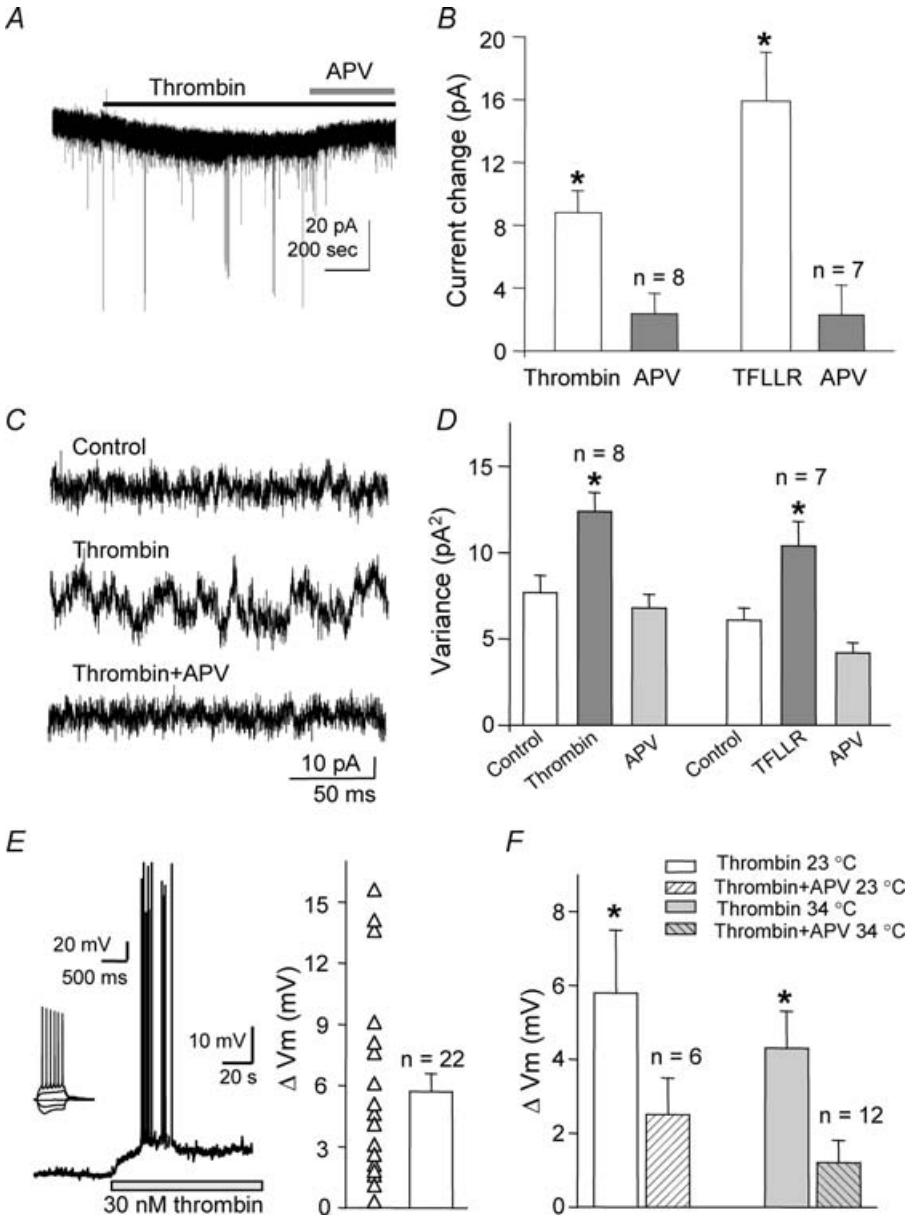

Figure 8. PAR1 activation induces an inward current and a depolarization in hippocampal CA1 pyramidal cells

A, representative current trace showing 30 nM thrombin-induced inward current in a CA1 pyramidal cell in a hippocampal slice. The inward current was abolished by switching to thrombin plus 100 μM APV. Recording was performed at −60 mV in the presence of 0.5 μM TTX and 5 μM Mg^{2+}. *B*, summary of amplitude changes of inward current induced by thrombin and TFLLR with and without coapplication of APV: thrombin 8.8 ± 3.1 pA, thrombin + APV 2.4 ± 1.3 pA; TFLLR 15.9 ± 3.1 pA, TFLLR + APV 2.3 ± 1.9 pA. $^*P < 0.05$, 1-factor repeated measures ANOVA with Dunnett's test. *C*, application of thrombin (30 nM) induces an increase in membrane current variance in the presence of TTX and the presence of low external Mg^{2+}, which is blocked by 100 μM APV. mEPSCs were digitally removed as described in the Methods. *D*, summary of membrane current variance measurements from CA1 pyramidal cells held under voltage clamp (−60 mV) by thrombin (control 7.7 ± 1.0 pA^2; thrombin 12.4 ± 1.1 pA^2; thrombin + APV 6.8 ± 2.3 pA^2) and the PAR1 agonist peptide TFLLR (30 μM; control 6.1 ± 0.7 pA^2; TFLLR 10.4 ± 1.4 pA^2; TFLLR + APV 4.2 ± 0.6 pA^2); $^*P < 0.05$; 1-factor repeated measures ANOVA with Dunnett's test. *E*, current clamp recording from a CA1 pyramidal cell (left panel) showing depolarization and spike firing during application of 30 nM thrombin (1.5 mM Mg^{2+}). Inset shows spike firing during depolarizing current injection. Right panel is the summary of current clamp recordings from 22 neurones showing a significant depolarization of the membrane potential ($P < 0.01$; paired *t* test). *F*, APV (100 μM) significantly reduces thrombin-mediated depolarization of the membrane potential at 23°C (thrombin 5.8 ± 1.7 mV; thrombin + APV 2.5 ± 1.0 mV, $n = 6$) and at 34°C (thrombin 4.3 ± 1.0 mV; thrombin + APV 1.2 ± 0.6 mV, $n = 12$), $^*P < 0.05$, 1-factor repeated measures ANOVA with Dunnett's test.

electrotonic distances from the somatic recording site to the synapses giving rise to mEPSCs (Rall, 1962; Stricker *et al.* 1996; Smith *et al.* 2003). Two subgroups of mEPSCs were selected for analysis based on the rise time, as shown in the rise time distribution (Fig. 10*B*). The first group possessed a rise time of 1–5 ms, whereas the second group showed a slow rise time (5–10 ms). Inward currents with rise times slower than 10 ms were rare, which probably reflected poorly clamped EPSCs subject to heavy electrotonic filtering, and thus were not analysed. Application of 30 μM TFLLR to selectively activate PAR1 had no significant effects on the frequency (data not shown), time course, or amplitude of mEPSCs with faster rise time (< 5 ms), assumed to arise from more proximal synapses under relatively good voltage control (Fig. 10*C* and *D*). By contrast, application of TFLLR markedly prolonged the decay of the average time course for slow rising mEPSCs recorded in the presence of extracellular Mg^{2+} compared to control mEPSCs; there was no significant change in the frequency or peak amplitude (Fig. 10*E*). The prolonged time course was manifested as an appearance of a second slow decay time constant in the presence of TFLLR (Fig. 10*F*). This TFLLR-dependent slow component of the mEPSC decay was sensitive to the NMDA receptor blocker APV (50 μM; Fig. 10*F*), whereas the average peak amplitude and frequency of mEPSCs were unaffected by APV. Average responses were analysed because the activity of only a few channels in individual mEPSCs is stochastic, and thus exponential waveforms, while adequately describing macroscopic averages, cannot be fitted to individual mEPSCs (Bekkers & Stevens, 1989; Silver *et al.* 1992). These data suggest that application of TFLLR allowed the NMDA component of the mEPSC, which is normally inhibited by 1.5 mM Mg^{2+}, to become

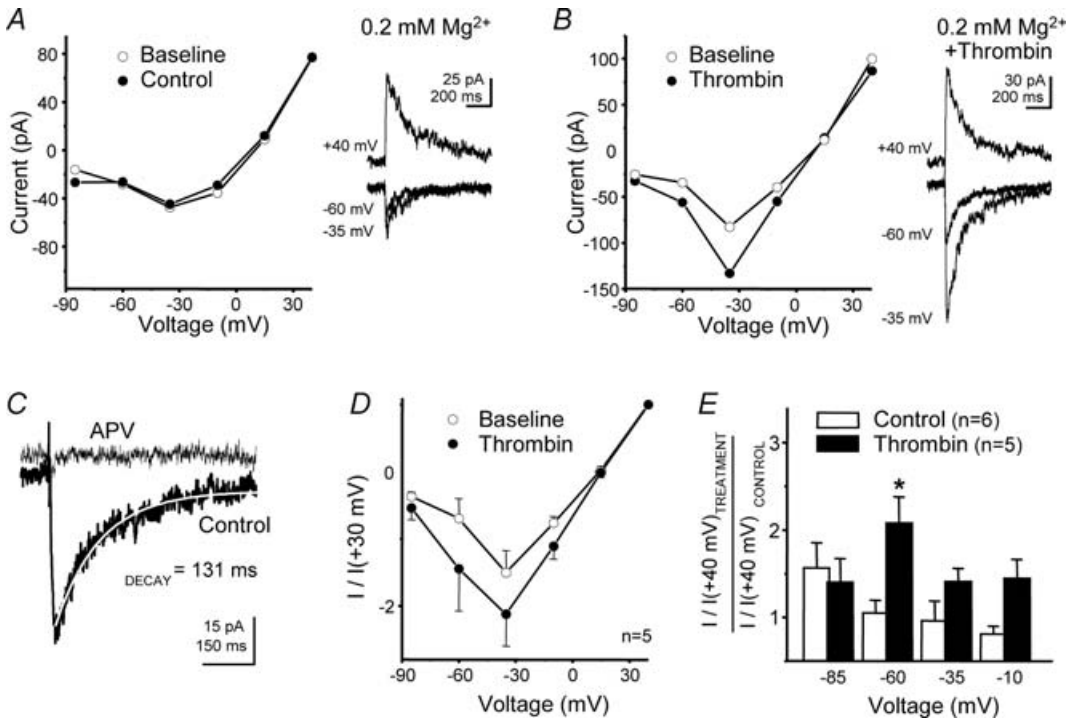

Figure 9. PAR1 activation reduces Mg^{2+} block of synaptic NMDA receptors
A, the current voltage (*I–V*) relation for evoked NMDA EPSCs was recorded at 5 min intervals from CA1 pyramidal cells under voltage clamp at the indicated membrane potential. Slices were bathed in 10 μM CNQX and 20 μM bicuculline. External Mg^{2+} was reduced to 0.2 mM to allow visualization of the NMDA component. The peak current is plotted as a function of holding potential before (labelled Baseline) and after (labelled Control) changing to perfusion with 0.2 mM Mg^{2+} ACSF from a different reservoir to control for mechanical artefacts. The inset shows the traces at the indicated holding potential. *B*, peak current is plotted as a function of membrane potential from a CA1 pyramidal cell before and 12.5 min following treatment with 30 nM thrombin. Right panel shows the traces at indicated holding potential. *C*, evoked EPSCs were blocked by the competitive NMDA receptor antagonist D-APV (50 μM), confirming they were mediated by NMDA receptors. *D*, two *I–V* curves were pooled before (2.5–12.5 min; ○, labelled Baseline) and during (7.5–12.5 min •) treatment with 30 nM thrombin. *I–V* curves were normalized to the current at +40 mV for each cell, and averaged across all cells. There was no change in membrane resistance (1.0 GΩ) or series resistance over the course of the experiment. *E*, the relief of Mg^{2+} block for thrombin-treated cells was compared to that for control cells as the indicated ratio. $^*P < 0.05$, Mann–Whitney test.

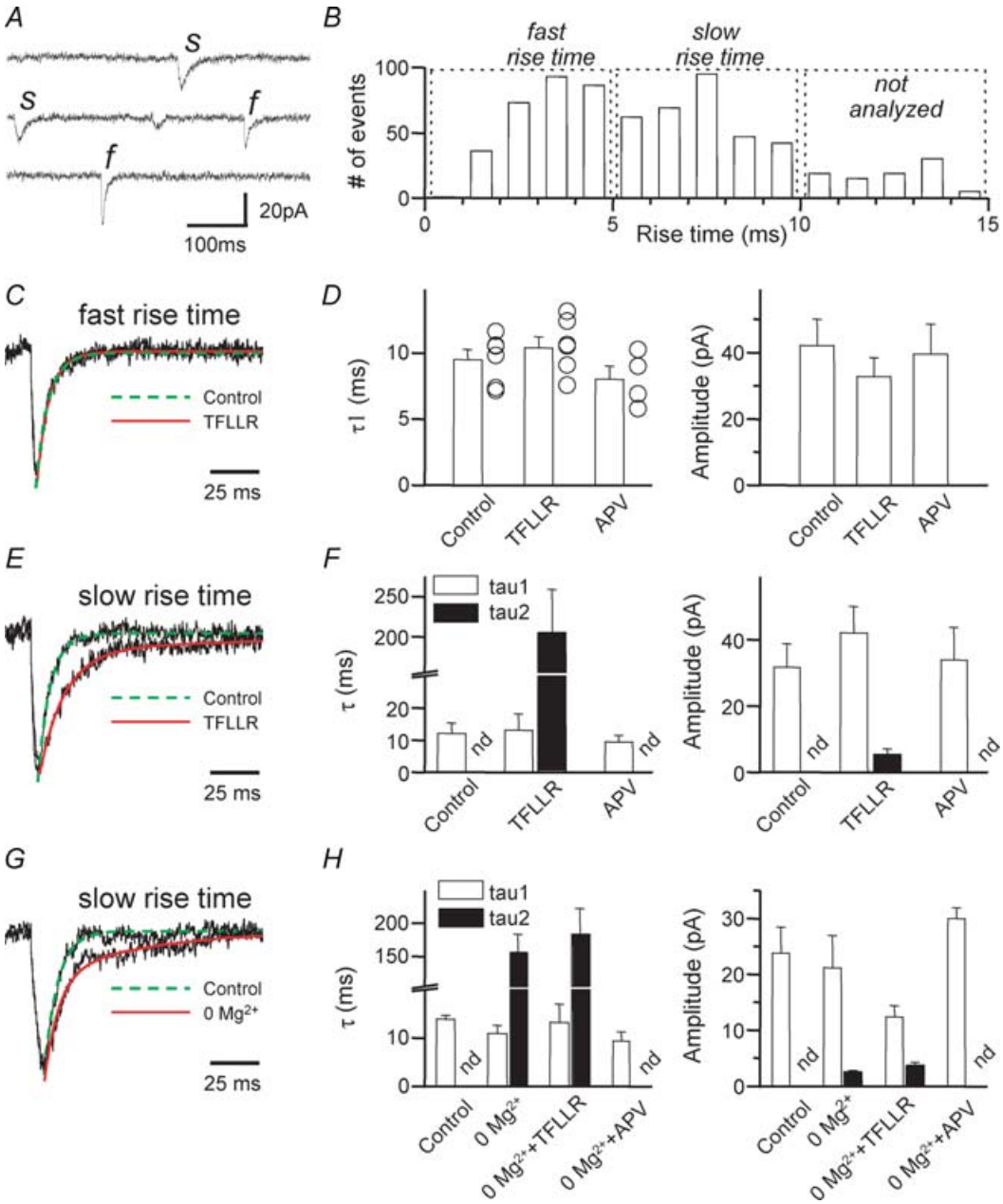

Figure 10. PAR1 activation potentiates the NMDA receptor component of mEPSCs in CA1 pyramidal neurones

A, three selected traces show the different rise times of mEPSCs recorded under voltage clamp from CA1 pyramidal cells in hippocampal slices in 0.5 μM TTX (*f* and *s* stand for fast rise and slow rising mEPSCs, respectively). *B*, histogram of the 10–90% rise times of 692 mEPSCs recorded from 11 cells for 5 min. *C*, superimposed normalized average traces are shown for fast rising mEPSCs in the absence and presence of TFLLR. The average traces were best fitted with a single component exponential function, shown in green for control and red for TFLLR, which superimpose. *D*, bar graph showing no significant difference in the decay time constant τ_1 (left panel) or amplitude (right panel) of fast rising mEPSCs recorded under control conditions or during application of TFLLR or APV (50 μM, $P > 0.05$, 1-factor repeated measures ANOVA with Dunnett's test). *E*, the superimposed normalized average traces are shown for slow rising mEPSCs from the same cell as in *D* in the absence and presence of TFLLR. The average traces were best fitted with a single component exponential function (control, green) or a two component exponential function (TFLLR, red). Activation of PAR1 by TFLLR induced the appearance of a slowly decaying synaptic current. *F*, bar graph showing no significant difference in the decay time constant τ_1 (left panel) or amplitude (right panel) of the fastest component of mEPSCs recorded under all conditions ($P > 0.05$, 1-factor repeated measures ANOVA with Dunnett's test). By contrast, a second slower decay time constant ($\tau_2 = 205 \pm 54$ ms, $n = 6$) was evident only after TFLLR treatment. APV eliminated the TFLLR-induced slow component (labelled τ_2, $P < 0.05$, paired *t* test); 'nd' indicates that the second slow exponential component (τ_2) was not detected. *G*, the superimposed normalized

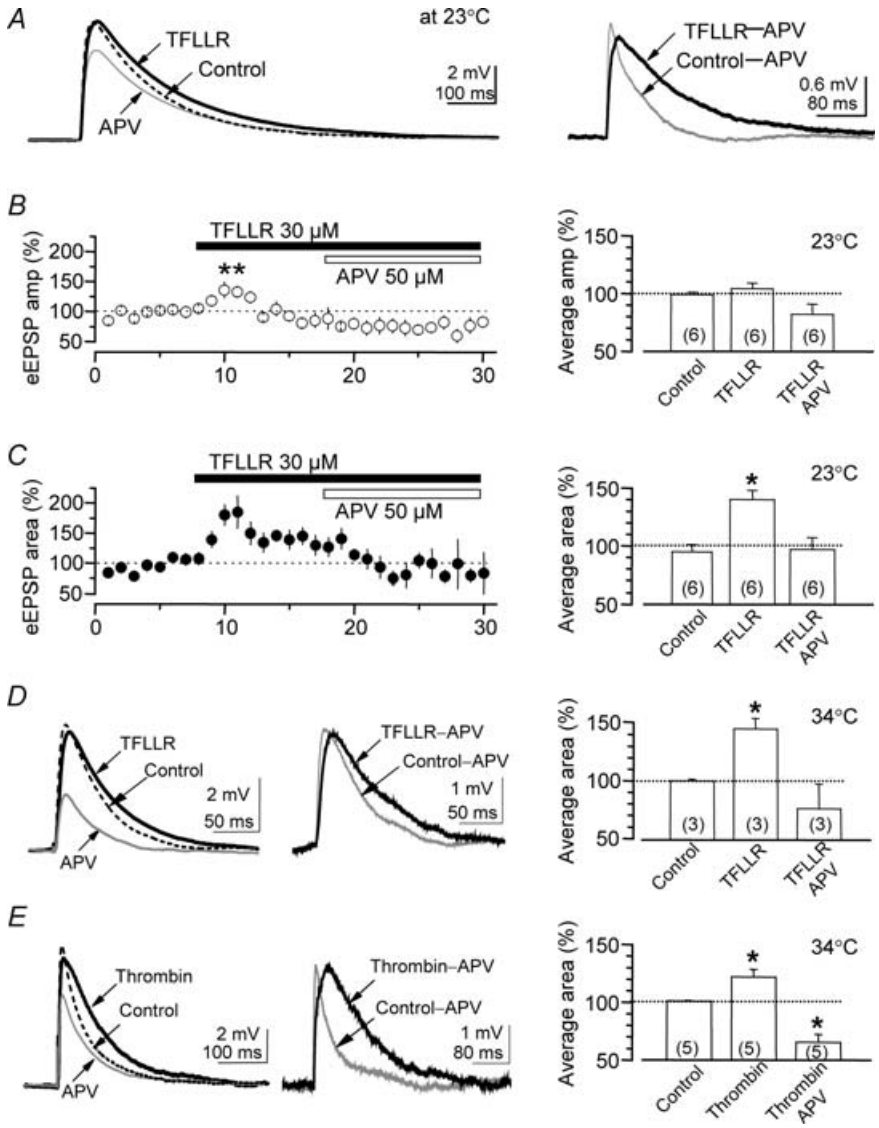

Figure 11. PAR1 activation potentiates the NMDA receptor component of evoked EPSPs in CA1 pyramidal cells

A, average EPSP is shown from a single representative rat CA1 pyramidal cell before (dashed black line) and during application of the PAR1 agonist TFLLR (continuous black line, 30 μM). The EPSP in the presence of APV is shown in grey. Right panel shows the difference potential between the EPSP recorded under control and APV, or between TFLLR and APV. Note the enhancement of the late phase of the EPSP by PAR1 activation. *B*, the average time course of the peak amplitude is shown during application of 30 μM TFLLR; error bars are S.E.M. Right panel shows TFLLR activation of PAR1 has no significant effect on the overall amplitude of the EPSP ($P > 0.05$, 1-factor repeated measures ANOVA with Dunnett's test) although there is a significant difference at an early time point marked by asterisks on left panel; number in parentheses is the number of cells. *C*, the average time course of the area under the EPSP is shown during application of the PAR1 activator TFLLR (30 μM) and APV (100 μM). The right panel shows that TFLLR significantly enhances the area of the EPSP, consistent with an enhancement of the NMDA component. The enhancement is blocked by 100 μM APV (*$P < 0.05$, 1-factor repeated measures ANOVA with Dunnett's test). *D* and *E*, the potentiation of synaptic NMDA component of EPSPs by PAR1 activation (TFLLR by 145 ± 9%, and thrombin: 120 ± 6%) is also observed near physiological temperature (34°C; *$P < 0.05$, 1-factor repeated measures ANOVA with Dunnett's test).

average traces shown for slow rising mEPSCs possessed a slow NMDA receptor-mediated component in nominal absence of extracellular Mg^{2+}. *H*, TFLLR had no significant effect on fitted time constants or amplitudes of the two synaptic components in Mg^{2+} free ACSF ($P > 0.05$, 1-factor repeated measures ANOVA with Dunnett's test). APV eliminated the slowest component in the absence of Mg^{2+}, confirming that it was mediated by NMDA receptors ($P < 0.05$, 1-factor repeated measures ANOVA with Dunnett's test).

prominent, consistent with our working hypothesis. Interestingly, the increase in decay time was only observed in the mEPSCs with a slower rise time (> 5 ms), which we interpret to represent quantal events arising at distal synapses at which the voltage clamp is less effective, thus allowing PAR1-mediated depolarization.

We subsequently tested the role of extracellular Mg^{2+} on PAR1 potentiation of NMDA receptor function by removing Mg^{2+} from the extracellular solution. Under this condition, control mEPSCs showed a prominent and slow NMDA receptor-mediated synaptic component (Fig. 10*G*). Application of 30 μM TFLLR had no significant effect on either the slow decay time constant or the fitted amplitude of the NMDA component in the absence of Mg^{2+} (Fig. 10*H*; $P > 0.05$, paired t test). These data indicate that extracelllular Mg^{2+} is required for the PAR1 potentiation of postsynaptic NMDA receptors. This increase of the NMDA receptor component of distal but not proximal mEPSCs along with the Mg^{2+} dependence suggests that PAR1-induced potentiation of NMDA receptors involves depolarization of the distal dendrites that in turn causes a relief of synaptic Mg^{2+} block. If extracellular Mg^{2+} is removed and there is no voltage-dependent block of NMDA receptors, than the distal depolarization will not lead to any potentiation of the unblocked NMDA receptors.

Astrocytic PAR1-mediated glutamate release enhances synaptic NMDA receptor potentials in slices

Our working hypothesis is that the dendritic depolarization occurs secondary to PAR1-mediated release of glutamate from astrocytes. The voltage clamp data above suggests that depolarization-mediated relief of Mg^{2+} blockade of synaptic NMDA receptors can be detected preferentially at distal synapses that are under poor voltage clamp. However, if our working hypothesis is correct, the use of voltage clamp is a suboptimal technique for evaluating the effects of PAR1 activation on synaptic NMDA receptors, since only poorly clamped synapses will be responsive to PAR1 activation. We therefore carried out a series of current clamp experiments to directly measure the effects of PAR1 activation on the NMDA receptor-mediated component of the EPSP recorded in the presence of 1.5 mM Mg^{2+}. We included QX314 in the intracellular pipette solution to block action potentials in the recorded neurone, and also included 10 μM bicuculline in the extracellular solution. A surgical cut was made between the CA3 and CA1 regions to prevent polysynaptic feedback inhibition and excitation from contaminating the EPSP waveform. Application of a 0.1 ms 1–100 μA stimulus to the Schaffer collaterals with a bipolar electrode evoked a monosynaptic EPSP that rapidly rose to a mean amplitude of 3.7 ± 0.9 mV (Fig. 11*A*; $n = 6$). The EPSP decayed with a slow time course ($\sim\tau_{decay}$ 65 ms), consistent with its being a dual AMPA and NMDA receptor-mediated EPSP, as expected following the reduction of feedback inhibition (Collingridge *et al.* 1988). When 30 μM TFLLR was applied to the slices, the late phase of the EPSP appeared to be potentiated, as shown by comparison of the difference potential between EPSPs recorded under control conditions and APV or between TFLLR and APV (Fig. 11*A*). There was no significant effect on the amplitude of the EPSP after a modest and transient potentiation (asterisk in Fig. 11*B*). By contrast, TFLLR-mediated PAR1 activation significantly increased charge transfer calculated from the integral (i.e. area) of the EPSP to $140 \pm 8\%$ of control (Fig. 11*C*; $n = 6$; $P < 0.05$). Application of 50 μM APV reversed this potentiation by TFLLR at the conclusion of the experiment. To confirm that the astrocytic release of glutamate that appears to depolarize neurones at 23°C also occurs under more physiological conditions with robust glutamate uptake, we repeated the experiment in slices at 34°C. Figure. 11*D* and *E* shows that both 30 μM TFLLR and 30 nM thrombin potentiate the APV sensitive component of the EPSP recorded at 34°C. These data confirm that both activators of thrombin are effective at enhancing the NMDA component of EPSPs, and that the effects occur under near physiological conditions (34°C).

Discussion

The most important finding of this study is that an astrocytic Gαq/11-coupled receptor (e.g. PAR1) can evoke Ca^{2+}-dependent glutamate efflux that subsequently controls postsynaptic NMDA receptor function in neurones. Our working hypothesis is that the PAR1-triggered glutamate efflux from astrocytes depolarizes adjacent neurones through activation of NMDA receptors, which have a ~100-fold lower EC_{50} than AMPA or kainate receptors (Dingledine *et al.* 1999). This hypothesized astrocyte-induced depolarization of neurones relieves voltage-dependent Mg^{2+} block of synaptic NMDA receptors to potentiate subsequent synaptic NMDA receptor-mediated EPSPs (Fig. 12*A*). This hypothesis is consistent with a wide range of data and emphasizes the critical role of astrocyte–neurone communication in the control of synaptic function (reviewed by Haydon, 2001; Nedergaard *et al.* 2002; Zhang & Haydon, 2005). Moreover, it supports the idea that a number of G-protein-coupled receptors that elevate intracellular Ca^{2+} in astrocytes and stimulate glutamate release (e.g. P2Y, bradykinin B2 receptors, prostaglandin E1 receptors – Parpura *et al.* 1994; Bezzi *et al.* 1998; Jeremic *et al.* 2001; Fellin *et al.*

2004) could potentiate NMDA receptor-mediated synaptic potentials by a similar mechanism. These data additionally suggest that other mechanisms that trigger increases in intracellular astrocytic Ca^{2+} (such as activation of Ca^{2+} waves; Cornell-Bell *et al.* 1990) could similarly control the NMDA-component of synaptic transmission. Moreover, this mechanism might also account for some forms of potentiation of NMDA receptor function by Gαq/11 coupled receptors for which no mechanism has been described (e.g. Mannaioni *et al.* 2001).

How much glutamate release might be needed to relieve voltage-dependent block of NMDA receptors? The answer to this question requires detailed modelling studies that take into account receptor properties, synaptic glutamate levels, glutamate uptake kinetics, kinetics of voltage-dependent block, and a detailed understanding of the electrotonic properties of spine heads and channel densities therein. Although such an analysis is beyond the scope of the present study, we can still consider a rough estimation of NMDA receptors from information in the literature. For example, Turner (1984) suggested that an integrated conductance of 1200 pS ms can produce at most 20 mV spine depolarization for a minimum spine neck diameter, which is sufficient to relieve Mg^{2+} blockade. Interestingly, only ∼0.1 mV somatic depolarization is observed, illustrating why spine depolarization could effectively relieve synaptic Mg^{2+} block without causing profound somatic depolarization. Starting from this result, we can use the integral of an exponential function (i.e. the product of the amplitude and time constant) to estimate the number of NMDA receptors needed to generate 1200 pS ms following a hypothetical transient astrocytic

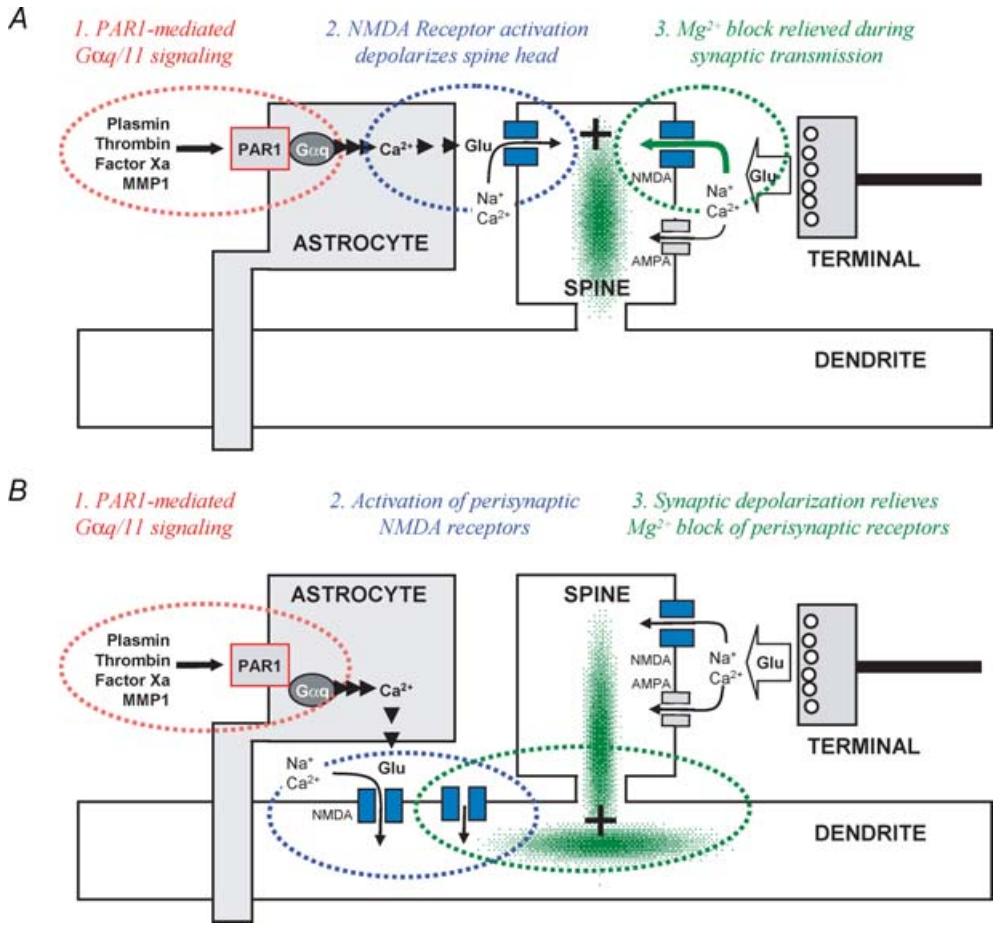

Figure 12. Mechanism for potentiation of synaptic NMDA receptor function by astrocytic PAR1 activation

A, the diagram illustrates how PAR1 activation in astrocytes subsequently leads to potentiation of synaptic NMDA receptor responses secondary to glutamate-mediated spine head depolarization (green) and reduction in Mg^{2+} block of synaptic NMDA receptors. *B*, diagram illustrates how sustained release of glutamate from astrocytes following PAR1 activation could lead to tonic activation of perisynaptic NMDA receptors. These receptors would remain blocked by Mg^{2+} until EPSPs in adjacent synapses lead to significant dendritic depolarization (green). The resulting unblock of perisynaptic NMDA receptors during dendritic depolarization would appear as a boost of the NMDA receptor component of the EPSP.

release of glutamate. If the time constant describing the current relaxation is ∼50 ms for NR1/NR2A deactivation following a pulse of glutamate released from astrocytes near the spine, then a transient synaptic-like NMDA receptor peak response of 24 pS is needed to produce a 20 mV depolarization within a spine head. If unitary conductance is ∼50 pS and open probability is ∼0.5 (Erreger *et al.* 2005) this could be produced by a single NMDA receptor in the absence of Mg^{2+}, or perhaps 20 or more receptors in the presence of 1.5 mM Mg^{2+}. Fewer receptors would be required if glutamate release lasted for a few seconds. A recent evaluation of dendritic NMDA receptor activation (Rhodes, 2006) provides an estimate of how many dendritic peri-synaptic NMDA receptors would be required to depolarize dendrites, and thus spines if we assume current spread into spine heads. A ∼5 nS conductance change applied to a dendritic shaft produces ∼25 mV depolarization. In the absence of Mg^{2+} this would correspond to 200 NR1/NR2A receptors (open probability 0.5, conductance 50 pS). In 1.5 mM Mg^{2+}, perhaps 4000 channels would need to be activated. In both cases, similar numbers of NR1/NR2B receptors would be needed because the 5-fold slower relaxation is offset by the 5-fold lower open probability. Although rough approximations such as these cannot determine how many receptors are needed to trigger depolarization-induced relief of Mg^{2+} block, they illustrate the importance of receptor localization as well as detailed and comprehensive analysis of spine head biophysics and electrotonic processing of information.

Relation of results to previous studies

Our data identify a new astrocytic receptor (PAR1) that is capable of releasing glutamate, consistent with previous studies on bradykinin, P2Y, and prostaglandin E2 (Parpura *et al.* 1994; Bezzi *et al.* 1998; Jeremic *et al.* 2001). These results support our interpretation that the mechanisms described here are likely to transfer to other receptor systems, and thus have broad implications. Although blood-derived thrombin and plasmin are normally excluded from the CNS by the blood–brain barrier, these two well known activators of PAR1 are expressed in brain parenchyma (Festoff *et al.* 1992; Basham & Seeds, 2001; Pang *et al.* 2004; Arai *et al.* 2006). The physiological role of PAR1 receptors in normal synaptic transmission remains unknown, in part because there is as yet no comprehensive understanding of conditions under which brain derived protease release is regulated. Interestingly, tissue plasminogen activator (tPA), which is known to convert plasminogen to plasmin, has been shown to contribute to long-term potentiation, an NMDA receptor-dependent cellular model of learning and memory (Baranes *et al.* 1998). Several lines of evidence suggest that the plasmin system can influence NMDA receptor-dependent cellular and behavioural models of learning and memory (Nakagami *et al.* 2000; Pawlak *et al.* 2002, 2005; Nagai *et al.* 2004, 2006; Pang *et al.* 2004); similarly, PAR1−/− mice show deficiencies in emotional learning, an NMDA receptor dependent process (Almonte *et al.* 2007). These results together with data showing activation of PAR1 following tPA cleavage of endogenous plasminogen (Junge *et al.* 2003) suggest that plasmin could be an endogenous ligand for PAR1, and may tune the NMDA receptor function in a manner relevant for synaptic plasticity and behaviour. Our data suggest that localized activation of PAR1 could induce release of micromolar glutamate that enhances the NMDA receptor activity in spines of neighbouring neurones, thus boosting the NMDA component of synaptic transmission. By potentiating synaptic NMDA receptor function, we predict that PAR1 activation would decrease threshold for stimuli needed to trigger changes in synaptic strength. In addition to activation of PAR1 by endogenous brain derived proteases under normal conditions, high concentrations of thrombin can enter brain parenchyma during blood–brain barrier breakdown in a wide range of pathological situations or during neurosurgery (Gingrich & Traynelis, 2000). Thus, our demonstration that an endogenous activator of PAR1 (thrombin) can potentiate synaptic NMDA receptor function raises the possibility that the mechanisms described here can be engaged by thrombin extravasation into brain during injury or neuropathological insult.

Even though the Ca^{2+}-dependent release of glutamate from astrocytes is now a well-established phenomenon, both the precise mechanism and physiological roles are still debated (reviewed in Nedergaard *et al.* 2002). Two classes of mechanisms that have been proposed for astrocytic glutamate release including regulated exocytosis (Bezzi *et al.* 1998; Araque *et al.* 2000; Pasti *et al.* 2001; Fellin *et al.* 2004) and channel-mediated release (Nedergaard *et al.* 2002). At least three channels including $P2X_7$ receptors (Duan *et al.* 2003), gap junction hemichannels (Ye *et al.* 2003), and volume sensitive anion channels (Kimelberg *et al.* 1990; Junankar & Kirk, 2000) have been suggested to allow Ca^{2+}-independent glutamate release through permeation. More work will be required to determine which of the available Ca^{2+}-dependent pathways that lead to glutamate release are engaged by PAR1 activation.

A number of studies have suggested that glutamate released from astrocytes is capable of activating ionotropic or metabotropic glutamate receptors on neurones (e.g. Parpura *et al.* 1994; Fellin *et al.* 2004; Wirkner *et al.* 2007). Furthermore, in a recent report, activation of neuronal metabotropic glutamate receptors by astrocytic glutamate release has been proposed to potentiate NMDA receptor function (Wirkner *et al.* 2007). Our findings, are fully consistent with this body of work, with the

exception that the low level of neuronal NMDA receptor activation following astrocytic PAR1-mediated release of glutamate appears to potentiate synaptic NMDA receptor responses by a Mg^{2+}-dependent mechanism rather than intraneuronal post-translational modification. The data described here suggest that any potential neuronal depolarization mediated by dendritic NMDA receptors in response to astrocytic glutamate release, regardless of the mechanism of release, may be capable of reducing Mg^{2+}-dependent block and potentiating the NMDA receptor component of EPSPs. Although numerous studies have shown levels of PAR1 activators in CNS tissue that are capable of potentiating NMDA receptors through PAR1 (see above), the potentiation described here should not be specific to PAR1. A large number of Gαq/11 coupled receptors are expressed by mammalian astrocytes, and we predict that many of these might be able to engage the proposed mechanism.

One key finding of these experiments is that the level of glutamate estimated to be released from astrocytes ($\sim$1 μM) following PAR1 activation is much lower than that in conventional neuronal synapses; intracleft glutamate has been estimated to reach 1 mM during vesicular release (Clements *et al.* 1992). Even if our estimation is off by severalfold, the extracellular concentration would still be sufficient to activate NMDA receptors, but insufficient to activate AMPA receptors. Activation of P2Y receptors has also been recently shown to potentiate NMDA receptor responses (Wirkner *et al.* 2007), which was suggested to involve glutamate release and activation of mGluR5. Our data are consistent with this interpretation, since ATP stimulates release of glutamate at levels ($\sim$6 μM) that could directly activate mGluR5 (glutamate EC_{50} at group I mGluRs 10 μM; Abe *et al.* 1992). By contrast, PAR1-mediated glutamate release from astrocyte seems less likely to engage mGluR activation because our estimations of glutamate concentrations following activation of PAR1 (1 μM) are well below reported EC_{50} value (10 μM) for glutamate activating recombinant group I metabotropic glutamate receptors.

Caveats and alternative hypotheses

There are at least two caveats to our working hypothesis. First, we have not shown direct biochemical evidence that glutamate is released from astrocytes in tissue slices. However, the data we present showing glutamate release from acutely dissociated CA1 astrocytes expressing GFP driven by the GFAP promoter creates a compelling argument that this occurs in brain tissue. Furthermore, by a wide range of measures, PAR1 signalling appears absent in CA1 pyramidal cells. Moreover, PAR1 activators are unable to evoke glutamate release from neurones. This further supports the idea that APV-sensitive currents observed in slices reflect release of glutamate from astrocytes. Second, one might predict that active glutamate uptake systems should blunt the levels of glutamate released by astrocytes, raising the question of how NMDA receptors get activated. Several pieces of data suggest that the glutamate release does indeed reach sufficient levels even in the presence of robust uptake to activate NMDA receptors. Most importantly, we find direct evidence that PAR1 activation can lead to APV-sensitive depolarization at 34°C, where uptake should occur at near physiological rates. In addition, we also note that the $\sim$1 μM glutamate we predicted to be present in our coculture system was detected in the narrow cleft between adjacent astrocytes and HEK cells, which will also be subject to some level of active astrocytic uptake.

Could activation of perisynaptic receptors in some way lead to amplification of the NMDA receptor component without direct spine head depolarization? Interestingly, one alternative hypothesis we have considered is that released glutamate might bind to and activate perisynaptic but not synaptic NMDA receptors (Fig. 12*B*). Under resting membrane potentials and normal levels of Mg^{2+}, these receptors would pass little current. However, upon depolarization, as occurs during synaptic transmission, the perisynaptic membrane potential may be reduced enough to relieve some of this block, leading to a boost of the NMDA receptor component as perisynaptic receptors supplement the synaptic NMDA receptors. For this mechanism to work, the voltage of the perisynaptic region would need to become sufficiently reduced to lead to receptor unblock during EPSPs. This alternative hypothesis is at least consistent with the data described in Figs 10 and 11, and cannot be ruled out as making a potential contribution to the results we observe. However, the direct depolarization (Fig. 8) and altered Mg^{2+} current–voltage curve (Fig. 9) suggest this mechanism is less likely to dominate the synaptic potentiation by astrocytic PAR1 activation.

Summary

In summary, the data described here support a potentially important mechanism of astrocyte-neuronal communication that is mediated by astrocytically released glutamate as well as a unique mechanism of NMDA receptor potentiation via relief of Mg^{2+} block. Our study provides strong evidence that astrocytes not only remove synaptically released glutamate, but also actively release glutamate in a Ca^{2+}-dependent fashion to shape the synaptic NMDA responses at nearby synapses. Our data further suggest that the mechanisms described here are likely to be shared by a range of astrocytic receptors.

References

Abe T, Sugihara H, Nawa H, Shigemoto R, Mizuno N & Nakanishi S (1992). Molecular characterization of a novel metabotropic glutamate receptor mGluR5 coupled to inositol phosphate/Ca^{2+} signal transduction. *J Biol Chem* **267**, 13361–13368.

Almonte AG, Hamill CE, Chhatwal JP, Wingo TS, Barber JA, Lyuboslavsky PN, Sweatt JD, Ressler KJ, White DA & Traynelis SF (2007). Mice lacking protease activated receptor-1 show deficits in emotional learning. *Neurobiology of Learning and Memory* (in press).

Anderson CM & Swanson RA (2000). Astrocyte glutamate transport: review of properties, regulation, and physiological functions. *Glia* **32**, 1–14.

Arai T, Miklossy J, Klegeris A, Guo JP & McGeer PL (2006). Thrombin and prothrombin are expressed by neurones and glial cells and accumulate in neurofibrillary tangles in Alzheimer disease brain. *J Neuropathol Exp Neurol* **65**, 19–25.

Araque A, Li N, Doyle RT & Haydon PG (2000). SNARE protein-dependent glutamate release from astrocytes. *J Neurosci* **20**, 666–673.

Bak LK, Schousboe A & Waagepetersen HS (2006). The glutamate/GABA-glutamine cycle: aspects of transport, neurotransmitter homeostasis and ammonia transfer. *J Neurochem* **98**, 641–653.

Banke TG, Bowie D, Lee H-K, Huganir RL, Schousboe A & Traynelis SF (2000). Control of GluR1 AMPA receptor function by cAMP-dependent protein kinase. *J Neurosci* **20**, 89–102.

Baranes D, Lederfein D, Huang YY, Chen M, Bailey CH & Kandel ER (1998). Tissue plasminogen activator contributes to the late phase of LTP and to synaptic growth in the hippocampal mossy fiber pathway. *Neurone* **21**, 813–825.

Basham ME & Seeds NW (2001). Plasminogen expression in the neonatal and adult mouse brain. *J Neurochem* **77**, 318–325.

Bekkers JM & Stevens CF (1989). NMDA and non-NMDA receptors are co-localized at individual excitatory synapses in cultured rat hippocampus. *Nature* **341**, 230–233.

Bekkers JM & Stevens CF (1995). Quantal analysis of EPSCs recorded from small numbers of synapses in hippocampal cultures. *J Neurophysiol* **73**, 1145–1156.

Bergles DE, Diamond JS & Jahr CE (1999). Clearence of glutamate inside the synapse and beyond. *Curr Opin Neurobiol* **9**, 293–298.

Bergles DE, Roberts JD, Somogyi P & Jahr CE (2000). Glutamatergic synapses on oligodendrocyte precursor cells in the hippocampus. *Nature* **11**, 187–191.

Bernatowicz MS, Klimas CE, Hartl KS, Peluso M, Allegretto NJ & Seiler SM (1996). Development of potent thrombin receptor antagonist peptides. *J Med Chem* **39**, 4879–4887.

Bezzi P, Carmignoto G, Pasti L, Vesce S, Rossi D, Rizzini BL, Pozzan T & Volterra A (1998). Prostaglandins stimulate calcium-dependent glutamate release in astrocytes. *Nature* **391**, 281–285.

Brenner M, Kisseberth WC, Su Y, Besnard F & Messing A (1994). GFAP promoter directs astrocyte-specific expression in transgenic mice. *J Neurosci* **14**, 1030–1037.

Clements JD, Lester RA, Tong G, Jahr CE & Westbrook GL (1992). The time course of glutamate in the synaptic cleft. *Science* **258**, 1498–1501.

Collingridge GL, Herron CE & Lester RAJ (1988). Synaptic activation of *N*-methyl-D-aspartate receptors in the Schaffer collateral–commisural pathway of rat hippocampus. *J Physiol* **399**, 283–300.

Connolly AJ, Ishihara H, Kahn ML, Farese RV Jr & Coughlin SR (1996). Role of the thrombin receptor in development and evidence for a second receptor. *Nature* **381**, 516–519.

Cornell-Bell AH, Finkbeiner SM, Cooper MS & Smith SJ (1990). Glutamate induces calcium waves in cultured astrocytes: long-range glial signaling. *Science* **247**, 470–473.

Coughlin SR (2000). Thrombin signalling and protease-activated receptors. *Nature* **407**, 258–264.

Coughlin SR (2001). Protease-activated receptors in vascular biology. *Thromb Haemost* **86**, 298–307.

D'Ambrosio R, Wenzel J, Schwartzkroin PA, McKhann GM 2nd & Janigro D (1998). Functional specialization and topographic segregation of hippocampal astrocytes. *J Neurosci* **18**, 4425–4438.

Danbolt NC (2001). Glutamate uptake. *Prog Neurobiol* **65**, 1–105.

Dingledine R, Borges K, Bowie D & Traynelis SF (1999). The glutamate receptor ion channels. *Pharmacol Rev* **51**, 7–61.

Duan S, Anderson CM, Keung EC, Chen Y, Chen Y & Swanson RA (2003). P2X7 receptor-mediated release of excitatory amino acids from astrocytes. *J Neurosci* **23**, 1320–1328.

Dzubay JA & Jahr CE (1999). The concentration of synaptically released glutamate outside of the climbing fiber-Purkinje cell synaptic cleft. *J Neurosci* **19**, 5265–5274.

Erreger K, Dravid SM, Banke TG, Wyllie DJA & Traynelis SF (2005). Subunit-specific gating controls rat NR1/NR2A and NR1/NR2B NMDA receptor kinetics and synaptic signalling profiles. *J Physiol* **552**, 335–344.

Esslinger C, Titus J, Koch H, Bridges R & Chamberlin A (2002). Methylation of 1-trans-2,4-pyrrolidine dicarboxylate converts the glutamate transport inhibitor from a substrate to a nonsubstrate inhibitor. *Bioorg Med Chem* **10**, 3509–3515.

Farinelli SE & Nicklas WJ (1992). Glutamate metabolism in rat cortical astrocyte cultures. *J Neurochem* **58**, 1905–1915.

Fellin T, Pascual O, Gobbo S, Pozzan T, Haydon PG & Carmignoto G (2004). Neuroneal synchrony mediated by astrocytic glutamate through activation of extrasynaptic NMDA receptors. *Neuron* **43**, 729–743.

Festoff BW, Rao JS & Chen M (1992). Protease nexin I, thrombin- and urokinase-inhibiting serpin, concentrated in normal human cerebrospinal fluid. *Neurology* **42**, 1361–1366.

Franke H, Krugel U, Grosche J, Heine C, Hartig W, Allgaier C & Illes P (2004). P2Y receptor expression on astrocytes in the nucleus accumbens of rats. *Neuroscience* **2004**, 431–441.

Gingrich MB, Junge CE, Lyuboslavsky P & Traynelis SF (2000). Potentiation of NMDA receptor function by the serine protease thrombin. *J Neurosci* **20**, 4582–4595.

Gingrich MB & Traynelis SF (2000). Serine proteases and brain damage – is there a link? *Trends Neurosci* **23**, 399–407.

Hamill CE, Goldshmidt A, Nicole O, Brat D & Traynelis SF (2005). Glial reactivity following damage: implications for scar formation and neuronal recovery. *Clin Neurosurg* **52**, 29–44.

Haydon PG (2001). Glia: listening and talking to the synapse. *Nat Rev Neurosci* **2**, 185–193.

Hollenberg MD, Saifeddine M, al-Ani B & Kawabata A (1997). Proteinase-activated receptors: structural requirements for activity, receptor cross-reactivity, and receptor selectivity of receptor-activating peptides. *Can J Physiol Pharmacol* **75**, 832–841.

Ikeda Y, Ueno A, Naraba H, Matsuki N & Oh-ishi S (2000). Intracellular Ca^{2+} increase in neuro2A cells and rat astrocytes following stimulation of bradykinin B2 receptor. *Jpn J Pharmacol* **84**, 140–145.

James C, Collison DJ & Duncan G (2005). Characterization and functional activity of thrombin receptors in the human lens. *Invest Ophthalmol Vis Sci* **46**, 925–932.

Jeremic A, Jeftinija K, Stevanovic J, Glavaski A & Jeftinija S (2001). ATP stimulates calcium-dependent glutamate release from cultured astrocytes. *J Neurochem* **77**, 664–675.

Junankar PR & Kirk K (2000). Organic osmolyte channels: a comparative view. *Cell Physiol Biochem* **10**, 355–360.

Junge CE, Lee CJ, Hubbard KB, Zhang Z, Olsen JJ, Hepler JR, Brat DJ & Traynelis SF (2004). Protease activated receptor-1 (PAR1) in human brain: localization and functional expression in astrocytes. *Exp Neurol* **188**, 94–103.

Junge CE, Sugawara T, Mannaioni G, Alagarsamy S, Conn PJ, Brat DJ, Chan PH & Traynelis SF (2003). The contribution of protease-activated receptor 1 to neuroneal damage caused by transient focal cerebral ischemia. *Proc Natl Acad Sci U S A* **100**, 13019–13024.

Kahan C, Seuwen K, Meloche S & Pouyssegur J (1992). Coordinate, biphasic activation of p44 mitogen-activated protein kinase and S6 kinase by growth factors in hamster fibroblasts. Evidence for thrombin-induced signals different from phosphoinositide turnover and adenylylcyclase inhibition. *J Biol Chem* **267**, 13369–13375.

Kawabata A, Saifeddine M, Al-Ani B, Leblond L & Hollenberg MD (1999). Evaluation of proteinase-activated receptor-1 (PAR1) agonists and antagonists using a cultured cell receptor desensitization assay: activation of PAR2 by PAR1-targeted ligands. *J Pharmacol Exp Ther* **288**, 358–370.

Kimelberg HK, Goderie SK, Higman S, Pang S & Waniewski RA (1990). Swelling-induced release of glutamate, aspartate, and taurine from astrocyte cultures. *J Neurosci* **10**, 1583–1591.

Kobayashi K, Fukuoka T, Yamanaka H, Dai Y, Obata K, Tokunaga A & Noguchi K (2006). Neurones and glial cells differentially express P2Y receptor mRNAs in the rat dorsal root ganglion and spinal cord. *J Comp Neurol* **498**, 443–454.

Longuemare MC & Swanson RA (1995). Excitatory amino acid release from astrocytes during energy failure by reversal of sodium-dependent uptake. *J Neurosci Res* **40**, 379–386.

Macfarlane SR, Seatter MJ, Kanke T, Hunter GD & Plevin R (2001). Proteinase-activated receptors. *Pharmacol Rev* **53**, 245–282.

Mannaioni G, Marino MJ, Valenti O, Traynelis SF & Conn PJ (2001). Metabotropic glutamate receptors 1 and 5 differentially regulate CA1 pyramidal cell function. *J Neurosci* **21**, 5925–5934.

Meli R, Raso GM, Cicala C, Esposito E, Fiorino F & Cirino G (2001). Thrombin and PAR-1 activating peptide increase iNOS expression in cytokine-stimulated C6 glioma cells. *J Neurochem* **79**, 556–563.

Mitrovic AD & Johnston GA (1994). Regional differences in the inhibition of L-glutamate and L-aspartate sodium-dependent high affinity uptake systems in rat CNS synaptosomes by L-trans-pyrrolidine-2,4-dicarboxylate, threo-3-hydroxy-D-aspartate and D-aspartate. *Neurochem Int* **24**, 583–588.

Nagai T, Ito M, Nakamichi N, Mizoguchi H, Kamei H, Fukakusa A, Nabeshima T, Takuma K & Yamada K (2006). The rewards of nicotine: regulation by tissue plasminogen activator-plasmin system through protease activated receptor-1. *J Neurosci* **26**, 12374–12383.

Nagai T, Yamada K, Yoshimura M, Ishikawa K, Miyamoto Y, Hashimoto K, Noda Y, Nitta A & Nabeshima T (2004). The tissue plasminogen activator-plasmin system participates in the rewarding effect of morphine by regulating dopamine release. *Proc Natl Acad Sci U S A* **101**, 3650–3655.

Nakagami Y, Abe K, Nishiyama N & Matsuki N (2000). Laminin degradation by plasmin regulates long-term potentiation. *J Neurosci* **20**, 2003–2010.

Nedergaard M (1994). Direct signaling from astrocytes to neurones in cultures of mammalian brain cells. *Science* **263**, 1768–1771.

Nedergaard M, Ransom B & Goldman SA (2003). New roles for astrocytes: redefining the functional architecture of the brain. *Trends Neurosci* **26**, 523–530.

Nedergaard M, Takano T & Hansen AJ (2002). Beyond the role of glutamate as a neurotransmitter. *Nat Rev Neurosci* **3**, 748–755.

Nicole O, Goldshmidt A, Sorensen SD, Sastre A, Lyuboslavsky P, Hepler JR, McKeon R & Traynelis SF (2005). The role of PAR-1 in glial scar formation after brain injury. *J Neurosci* **25**, 4319–4329.

Ogino Y, Tanaka K & Shimizu N (1996). Direct evidence for two distinct G proteins coupling with thrombin receptors in human neuroblastoma SH-EP cells. *Eur J Pharmacol* **316**, 105–109.

Pang PT, Teng HK, Zaitsev E, Woo NT, Sakata K, Zhen S, Teng KK, Yung WH, Hempstead BL & Lu B (2004). Cleavage of proBDNF by tPA/plasmin is essential for long-term hippocampal plasticity. *Science* **306**, 487–491.

Parpura V, Basarsky TA, Liu F, Jeftinija K, Jeftinija S & Haydon PG (1994). Glutamate-mediated astrocyte-neurone signalling. *Nature* **369**, 744–747.

Pasti L, Zonta M, Pozzan T, Vicini S & Carmignoto G (2001). Cytosolic calcium oscillations in astrocytes may regulate exocytotic release of glutamate. *J Neurosci* **21**, 477–484.

Pawlak R, Nagai N, Urano T, Napiorkowska-Pawlak D, Ihara H, Takada Y, Collen D & Takada A (2002). Rapid, specific and active site-catalyzed effect of tissue plasminogen activator on hippocampus-dependent learning in mice. *Neuroscience* **113**, 995–1001.

Pawlak R, Rao BS, Melchor JP, Chattarji S, McEwen B & Strickland S (2005). Tissue plasminogen activator and plasminogen mediate stress-induced decline of neuroneal and cognitive functions in the mouse hippocampus. *Proc Natl Acad Sci U S A* **102**, 18201–18206.

Porter JT & McCarthy KD (1997). Astrocytic neurotransmitter receptors in situ and in vivo. *Prog Neurobiol* **51**, 439–455.
Raiteri L, Schid G, Prestipino S, Raiteri M & Bonanno G (2001). Activation of a6 $GABA_A$ receptors on depolarized cerebellar parallel fibers elicit glutamate release through anion channels. *Neuropharmacology* **41**, 943–951.
Rall W (1962). Electrophysiology of a dendritic neurone model. *Biophys J* **2**, 145–167.
Rhodes P (2006). The properties and implications of NMDA spikes in neocortical pyramidal cells. *J Neurosci* **26**, 6704–6715.
Schipke CG, Boucsein C, Ohlemeyer C, Kirchhoff F & Kettenmann H (2002). Astrocyte Ca^{2+} waves trigger responses in microglial cells in brain slices. *FASEB J* **16**, 255–257.
Silver RA, Traynelis SF & Cull-Candy SG (1992). Rapid time-course miniature and evoked excitatory currents at cerebellar synapses in situ. *Nature* **355**, 163–166.
Smirnova IV, Vamos S, Wiegmann T, Citron BA, Arnold PM & Festoff BW (1998). Calcium mobilization and protease-activated receptor cleavage after thrombin stimulation in motor neurones. *J Mol Neurosci* **10**, 31–44.
Smith MA, Ellis-Davies GC & Magee JC (2003). Mechanism of the distance-dependent scaling of Schaffer collateral synapses in rat CA1 pyramidal neurones. *J Physiol* **548**, 245–258.
Smith-Swintosky VL, Zimmer S, Fenton JW 2nd & Mattson MP (1995). Protease nexin-1 and thrombin modulate neuroneal Ca^{2+} homeostasis and sensitivity to glucose deprivation-induced injury. *J Neurosci* **15**, 5840–5850.
Sorensen SD, Nicole O, Peavy RD, Montoya LM, Lee CJ, Murphy TJ, Traynelis SF & Hepler JR (2003). Common signaling pathways link activation of murine PAR-1, LPA, and S1P receptors to proliferation of astrocytes. *Mol Pharmacol* **64**, 1199–1209.
Stern-Bach Y, Russo S, Neuman M & Rosenmund C (1998). A point mutation in the glutamate binding site blocks desensitization of AMPA receptors. *Neurone* **21**, 907–918.
Stricker C, Field AC & Redman SJ (1996). Statistical analysis of amplitude fluctuations in EPSCs evoked in rat CA1 pyramidal neurones *in vitro*. *J Physiol* **490**, 419–441.
Striggow F, Riek-Burchardt M, Kiesel A, Schmidt W, Henrich-Noack P, Breder J, Krug M, Reymann KG & Reiser G (2001). Four different types of protease-activated receptors are widely expressed in the brain and are up-regulated in hippocampus by severe ischemia. *Eur J Neurosci* **14**, 595–608.
Suo Z, Citron BA & Festoff BW (2004). Thrombin: a potential proinflammatory mediator in neurotrauma and neurodegenerative disorders. *Curr Drug Targets Inflamm Allergy* **3**, 105–114.
Suo Z, Wu M, Ameenuddin S, Anderson HE, Zoloty JE, Citron BA, Andrade-Gordon P & Festoff BW (2002). Participation of protease-activated receptor-1 in thrombin-induced microglial activation. *J Neurochem* **80**, 655–666.
Traynelis SF & Wahl P (1997). Control of rat GluR6 glutamate receptor open probability by protein kinase A and calcineurin. *J Physiol* **503**, 513–531.
Turner DA (1984). Conductance transients onto dendritic spines in a segmental cable model of hippocampal neurones. *Biophys J* **46**, 85–96.
Volterra A, Bezzi P, Rizzini BL, Trotti D, Ullensvang K, Danbolt NC & Racagni G (1996). The competitive transport inhibitor 1-trans-pyrrolidine-2,4-dicarboxylate triggers excitotoxicity in rat cortical neurone-astrocyte co-cultures via glutamate release rather than uptake inhibition. *Eur J Neurosci* **8**, 2019–2028.
Wang X, Lou N, Xu Q, Tian GF, Peng WG, Han X, Kang J, Takano T & Nedergaard M (2006). Astrocytic Ca^{2+} signaling evoked by sensory stimulation in vivo. *Nat Neurosci* **9**, 816–823.
Wang H & Reiser G (2003). Thrombin signaling in the brain: the role of protease-activated receptors. *Biol Chem* **384**, 193–202.
Wang H, Ubl JJ & Reiser G (2002*a*). Four subtypes of protease-activated receptors, co-expressed in rat astrocytes, evoke different physiological signaling. *Glia* **37**, 53–63.
Wang H, Ubl JJ, Stricker R & Reiser G (2002*b*). Thrombin (PAR-1) -induced proliferation in astrocytes via MAPK involves multiple signaling pathways. *Am J Physiol Cell Physiol* **283**, C1351–C1364.
Weinstein JR, Gold SJ, Cunningham DD & Gall CM (1995). Cellular localization of thrombin receptor mRNA in rat brain: expression by mesencephalic dopaminergic neurones and codistribution with prothrombin mRNA. *J Neurosci* **15**, 2906–2919.
Wirkner K, Gunther A, Weber M, Guzman SJ, Krause T, Fuchs J, Koles L, Norenberg W & Illes P (2007). Modulation of NMDA receptor current in Layer V pyramidal neurones of the rat prefrontal cortex by P2Y receptor activation. *Cereb Cortex* **17**, 621–631.
Xi G, Reiser G & Keep RF (2003). The role of thrombin and thrombin receptors in ischemic, hemorrhagic and traumatic brain injury: deleterious or protective? *J Neurochem* **84**, 3–9.
Xiong ZG, Raouf R, Lu WY, Wang LY, Orser BA, Dudek EM, Browning MD & MacDonald JF (1998). Regulation of N-methyl-D-aspartate receptor function by constitutively active protein kinase C. *Mol Pharmacol* **54**, 1055–1063.
Ye ZC, Wyeth MS, Baltan-Tekkok S & Ransom BR (2003). Functional hemichannels in astrocytes: a novel mechanism of glutamate release. *J Neurosci* **23**, 3588–3596.
Yang Y, Akiyama H, Fenton JW 2nd & Brewer GJ (1997). Thrombin receptor on rat primary hippocampal neurones: coupled calcium and cAMP responses. *Brain Res* **761**, 11–18.
Zhang Q & Haydon PG (2005). Roles of gliotransmission in the nervous system. *J Neural Transm* **112**, 121–125.
Zhang J, Zhang J, Benovic JL, Sugai M, Wetzker R, Gout I & Rittenhouse SE (1995). Sequestration of a G-protein beta gamma subunit or ADP-ribosylation of Rho can inhibit thrombin-induced activation of platelet phosphoinositide 3-kinases. *J Biol Chem* **270**, 6589–6594.

Acknowledgements

This work was supported by NIH NS43875 (C.J.L.), NARSAD (G.M., S.F.T.), MH11623 (M.B.G.), NS39419 (S.F.T.), the Emory University Research Committee (S.F.T.), the Korea Research Foundation KRF-2005-070-C00096 (C.J.L.), and the Ente Cassa di Risparmio di Firenze, Italy (G.M.). We thank Anders

Kristensen for contributing data on the concentration effect curve for GluR1(L497Y) and Anna Goldshmidt for analysing the Fura-2 image data. We also thank Aristides Sastre, Polina Lyuboslavsky, and Phuong Le for excellent technical assistance. We thank Dr Shaun Coughlin for sharing PAR1−/− mice, and Dr Jan Pohl at the Emory University Microchemical Facilitiy for synthesizing PAR1 agonist and antagonist.

Supplemental material

Online supplemental material for this paper can be accessed at:
http://jp.physoc.org/cgi/content/full/jphysiol.2007.130377/DC1
and
http://www.blackwell-synergy.com/doi/suppl/10.1113/jphysiol.2007.130377